Title

Rotation-minimizing Euler-Rodrigues rigid-body motion interpolants

Journal

Computer Aided Geometric Design, 30(7)

ISSN

0167-8396

Authors

Farouki, Rida T

Han, Chang Yong

Dospra, Petroula

et al.

Publication Date

2013-10-01

DOI

10.1016/j.cagd.2013.03.001

Peer reviewed

Rotation-minimizing Euler-Rodrigues rigid-body motion interpolants

Rida T. Farouki
Department of Mechanical and Aerospace Engineering,
University of California, Davis, CA 95616, USA

Chang Yong Han
Department of Applied Mathematics, Kyung Hee University,
Yongin–si, Gyeonggi–do 446–701, SOUTH KOREA

Petroula Dospra and Takis Sakkalis
Mathematics Laboratory, Agricultural University of Athens,
75 Iera Odos, Athens 11855, GREECE

Abstract

A characterization for spatial Pythagorean–hodograph (PH) curves of degree 7 with rotation–minimizing Euler–Rodrigues frames (ERFs) is determined, in terms of one real and two complex constraints on the curve coefficients. These curves can interpolate initial/final positions $\mathbf{p}_i$ and $\mathbf{p}_f$ and orientational frames $(\mathbf{t}_i, \mathbf{u}_i, \mathbf{v}_i)$ and $(\mathbf{t}_f, \mathbf{u}_f, \mathbf{v}_f)$ so as to define a rational rotation–minimizing rigid body motion. Two residual free parameters, that determine the magnitudes of the end derivatives, are available for optimizing shape properties of the interpolant. This improves upon existing algorithms for quintic PH curves with rational rotation–minimizing frames (RRMF quintics), which offer no residual freedoms. Moreover, the degree 7 PH curves with rotation–minimizing ERFs are capable of interpolating motion data for which the RRMF quintics do not admit real solutions. Although these interpolants are of higher degree than the RRMF quintics, their rotation–minimizing frames are actually of lower degree (6 versus 8), since they coincide with the ERF. This novel construction of rational rotation–minimizing motions may prove useful in applications such as computer animation, geometric sweep operations, and robot trajectory planning.

Keywords: Pythagorean–hodograph curves; Euler–Rodrigues frame; rotation–minimizing frame; quaternions; Hopf map; spatial motion planning.

e–mail: farouki@ucdavis.edu, cyhan@khu.ac.kr, pdospra@aua.gr, stp@aua.gr

1 Introduction

The need to describe the orientation of a rigid body that moves along a curved spatial path $\mathbf{r}(t)$ is a basic problem in computer animation, the use of sweep operations in geometric design, path planning in robotics, and programming of CNC machines with rotary axes. This can be accomplished by invoking an orthonormal frame $(\mathbf{f}_1, \mathbf{f}_2, \mathbf{f}_3)$ embedded in the body to specify its orientation. The variation of such a frame is defined by its angular velocity $\boldsymbol{\omega}(t)$ according to the relations

$$\frac{\mathrm{d}\mathbf{f}_1}{\mathrm{d}t} = \boldsymbol{\omega} \times \mathbf{f}_1 \,, \qquad \frac{\mathrm{d}\mathbf{f}_2}{\mathrm{d}t} = \boldsymbol{\omega} \times \mathbf{f}_2 \,, \qquad \frac{\mathrm{d}\mathbf{f}_3}{\mathrm{d}t} = \boldsymbol{\omega} \times \mathbf{f}_3 \,.$$

A common requirement is that the frame vector $\mathbf{f}_1$ should coincide with the path tangent $\mathbf{t} = \mathbf{r}'/|\mathbf{r}'|$, while the normal–plane vectors $\mathbf{f}_2, \mathbf{f}_3$ should exhibit no instantaneous rotation about $\mathbf{f}_1$ — such *rotation–minimizing* motions are characterized [1] by the fact that the angular velocity satisfies $\boldsymbol{\omega} \cdot \mathbf{f}_1 \equiv 0$.

Numerical methods are often used [11, 14, 16, 15, 17, 18] to approximate rotation–minimizing frames, since in general the unit vectors $\mathbf{f}_1(t)$, $\mathbf{f}_2(t)$, $\mathbf{f}_3(t)$ do not admit a rational dependence on the curve parameter, even if $\mathbf{r}(t)$ is a polynomial or rational curve. In recent years, there has been greater interest in constructing special curves that do possess rational rotation–minimizing frames (RRMF curves) — such curves must be Pythagorean–hodograph (PH) curves [4], since only the PH curves have rational unit tangents.

The introduction [2] of the *Euler–Rodrigues frame* (ERF) was a key step in identifying the RRMF curves as subset of the spatial PH curves. The ERF $(\mathbf{e}_1(t), \mathbf{e}_2(t), \mathbf{e}_3(t))$ is a *rational* orthonormal frame, defined on any spatial PH curve $\mathbf{r}(t)$, such that $\mathbf{e}_1 = \mathbf{r}'/|\mathbf{r}'|$ is the curve tangent $\mathbf{t}$. The RRMF curves are those PH curves for which the component of the ERF angular velocity in the direction of $\mathbf{e}_1$ can be eliminated by imposing a rational normal–plane rotation on the frame vectors $\mathbf{e}_2(t)$, $\mathbf{e}_3(t)$ at each curve point [13]. The first RRMF curves were identified by Choi and Han [2], as PH curves of degree 7 for which the ERF is itself rotation–minimizing — such curves were shown to depend on 16 real parameters, and the interpolation of first–order Hermite data (initial/final points $\mathbf{p}_i, \mathbf{p}_f$ and tangents $\mathbf{t}_i, \mathbf{t}_f$) was briefly studied.

Subsequently, RRMF curves of degree 5 were characterized [5, 8] in terms of coefficient constraints in the quaternion and Hopf map representations for spatial PH curves, and their use in constructing rational rotation–minimizing rigid–body motions — that interpolate initial/final positions $\mathbf{p}_i$ and $\mathbf{p}_f$ and frames $(\mathbf{t}_i, \mathbf{u}_i, \mathbf{v}_i)$ and $(\mathbf{t}_f, \mathbf{u}_f, \mathbf{v}_f)$ — was studied in [9]. With these curves,

however, it was not possible to guarantee the existence of rotation–minimizing interpolants to arbitrary spatial motion data.

This study revisits the degree 7 curves with rotation–minimizing ERFs identified by Choi and Han [2], and derives a simpler characterization of them in terms of one real and two complex constraints on their coefficients. It is also shown that, unlike the RRMF quintics [9], these curves admit two free parameters in the interpolation of initial/final positions $\mathbf{p}_i$ and $\mathbf{p}_f$ and frames $(\mathbf{t}_i, \mathbf{u}_i, \mathbf{v}_i)$ and $(\mathbf{t}_f, \mathbf{u}_f, \mathbf{v}_f)$ by rational rotation–minimizing motions. The free parameters permit shape optimization of the motion interpolant, and make the existence of interpolants to arbitrary data highly probable. Although the curves are of higher degree than the RRMF quintics, their rational RMFs are actually of lower degree, since they are coincident with the ERF.

The plan for the remainder of this paper is as follows. After reviewing the definitions and key properties of PH curves and RRMF curves in Sections 2 and 3, the problem of characterizing those degree 7 PH curves whose ERFs are rotation–minimizing is considered in Section 4. In particular, it is shown that one real and two complex constraints on the curve coefficients suffice to identify these curves. In Section 5, this characterization is exploited to derive a system of four quadratic equations in four real variables, that embodies the rational rotation–minimizing rigid–body motion problem. Preliminary methods for solving this system, together with computed examples, are then presented in Section 6. Finally, Section 7 summarizes the key results of this paper, and identifies problems that deserve further investigation.

2 Spatial PH curves

The characteristic feature of a polynomial *Pythagorean–hodograph* (PH) *curve* $\mathbf{r}(t) = (x(t), y(t), z(t))$ is that its derivative $\mathbf{r}'(t) = (x'(t), y'(t), z'(t))$ satisfies

$$x'^2(t) + y'^2(t) + z'^2(t) \;=\; \sigma^2(t) \tag{1}$$

for some polynomial $\sigma(t)$. The *quaternion* and *Hopf map* forms [3, 6] are two alternative (equivalent) models for the construction of PH curves. The former generates a Pythagorean hodograph $\mathbf{r}'(t)$ from a quaternion[1] polynomial

$$\mathcal{A}(t) \;=\; u(t) + v(t)\,\mathbf{i} + p(t)\,\mathbf{j} + q(t)\,\mathbf{k} \tag{2}$$

[1]Calligraphic characters such as $\mathcal{A}$ are used to denote quaternions, their scalar (real) and vector (imaginary) parts being indicated by scal($\mathcal{A}$) and vect($\mathcal{A}$). Bold symbols denote either complex numbers or vectors in $\mathbb{R}^3$ — the meaning should be clear from the context.

and its conjugate $\mathcal{A}^*(t) = u(t) - v(t)\,\mathbf{i} - p(t)\,\mathbf{j} - q(t)\,\mathbf{k}$ through the product[2]

$$\begin{aligned}\mathbf{r}'(t) \;&=\; \mathcal{A}(t)\,\mathbf{i}\,\mathcal{A}^*(t) \;=\; [\,u^2(t) + v^2(t) - p^2(t) - q^2(t)\,]\,\mathbf{i} \\ &\quad + 2\,[\,u(t)q(t) + v(t)p(t)\,]\,\mathbf{j} \;+\; 2\,[\,v(t)q(t) - u(t)p(t)\,]\,\mathbf{k}\,. \end{aligned} \tag{3}$$

The latter generates a Pythagorean hodograph from complex polynomials

$$\boldsymbol{\alpha}(t) \;=\; u(t) + \mathrm{i}\,v(t)\,, \quad \boldsymbol{\beta}(t) \;=\; q(t) + \mathrm{i}\,p(t) \tag{4}$$

through the expression

$$\mathbf{r}'(t) \;=\; (|\boldsymbol{\alpha}(t)|^2 - |\boldsymbol{\beta}(t)|^2, 2\,\mathrm{Re}(\boldsymbol{\alpha}(t)\overline{\boldsymbol{\beta}}(t)), 2\,\mathrm{Im}(\boldsymbol{\alpha}(t)\overline{\boldsymbol{\beta}}(t)))\,. \tag{5}$$

The equivalence of (3) and (5) is seen by setting $\mathcal{A}(t) = \boldsymbol{\alpha}(t) + \mathbf{k}\,\boldsymbol{\beta}(t)$, where the imaginary unit i is identified with the quaternion basis element $\mathbf{i}$. It will be advantageous to simultaneously employ both representations (3) and (5) of spatial PH curves — see [4] for further details.

The quaternion polynomial (2) and the complex polynomials (4) may be specified in terms of the Bernstein basis

$$b_r^n(t) \;=\; \binom{n}{r}(1-t)^{n-r}t^r\,, \quad r = 0, \ldots, n$$

of degree n on $t \in [\,0, 1\,]$ as

$$\mathcal{A}(t) \;=\; \sum_{r=0}^{n} \mathcal{A}_r\, b_r^n(t)\,, \tag{6}$$

$$\boldsymbol{\alpha}(t) \;=\; \sum_{r=0}^{n} \boldsymbol{\alpha}_r\, b_r^n(t)\,, \qquad \boldsymbol{\beta}(t) \;=\; \sum_{r=0}^{n} \boldsymbol{\beta}_r\, b_r^n(t)\,, \tag{7}$$

where the coefficients are related by $\mathcal{A}_r = \boldsymbol{\alpha}_r + \mathbf{k}\,\boldsymbol{\beta}_r$ for $r = 0, \ldots, n$.

An *adapted* orthonormal frame $(\mathbf{f}_1, \mathbf{f}_2, \mathbf{f}_3)$ on a space curve $\mathbf{r}(t)$ employs the curve tangent $\mathbf{t} = \mathbf{r}'/|\mathbf{r}'|$ as the vector $\mathbf{f}_1$, while the vectors $\mathbf{f}_2, \mathbf{f}_3$ span the curve normal plane. The *Euler–Rodrigues frame* (ERF) is a *rational* adapted rational frame, defined on spatial PH curves [2]. In terms of the quaternion form (3), it is specified by

$$\mathbf{e}_1(t) = \frac{\mathcal{A}(t)\,\mathbf{i}\,\mathcal{A}^*(t)}{|\mathcal{A}(t)|^2}\,, \quad \mathbf{e}_2(t) = \frac{\mathcal{A}(t)\,\mathbf{j}\,\mathcal{A}^*(t)}{|\mathcal{A}(t)|^2}\,, \quad \mathbf{e}_3(t) = \frac{\mathcal{A}(t)\,\mathbf{k}\,\mathcal{A}^*(t)}{|\mathcal{A}(t)|^2}\,. \tag{8}$$

[2]Note that a product of the form $\mathcal{A}(t)\,\mathbf{i}\,\mathcal{A}^*(t)$ always generates a pure vector quaternion.

Here $\mathbf{e}_1$ is the curve tangent $\mathbf{t} = \mathbf{r}'/|\mathbf{r}'|$, while $\mathbf{e}_2$, $\mathbf{e}_3$ span the curve normal plane. The ERF is a useful "reference frame" for the identification of rational rotation–minimizing frames [2]. The ERF can also be defined in terms of the Hopf map form (5) as

$$\begin{aligned}
\mathbf{e}_1(t) &= \frac{\big(|\boldsymbol{\alpha}(t)|^2 - |\boldsymbol{\beta}(t)|^2, 2\,\mathrm{Re}\,(\boldsymbol{\alpha}(t)\overline{\boldsymbol{\beta}}(t)), 2\,\mathrm{Im}\,(\boldsymbol{\alpha}(t)\overline{\boldsymbol{\beta}}(t)) \big)}{|\boldsymbol{\alpha}(t)|^2 + |\boldsymbol{\beta}(t)|^2}\,, \\
\mathbf{e}_2(t) &= \frac{\big(-2\,\mathrm{Re}\,(\boldsymbol{\alpha}(t)\boldsymbol{\beta}(t)), \mathrm{Re}\,(\boldsymbol{\alpha}^2(t) - \boldsymbol{\beta}^2(t)), \mathrm{Im}\,(\boldsymbol{\alpha}^2(t) + \boldsymbol{\beta}^2(t)) \big)}{|\boldsymbol{\alpha}(t)|^2 + |\boldsymbol{\beta}(t)|^2}\,, \\
\mathbf{e}_3(t) &= \frac{\big(2\,\mathrm{Im}\,(\boldsymbol{\alpha}(t)\boldsymbol{\beta}(t)), -\mathrm{Im}\,(\boldsymbol{\alpha}^2(t) - \boldsymbol{\beta}^2(t)), \mathrm{Re}\,(\boldsymbol{\alpha}^2(t) + \boldsymbol{\beta}^2(t)) \big)}{|\boldsymbol{\alpha}(t)|^2 + |\boldsymbol{\beta}(t)|^2}\,.
\end{aligned}$$

3 Rational rotation-minimizing frames

Han [13] showed that the RRMF curves can be characterized in terms of the quaternion form (2)–(3) of spatial PH curves by the existence of relatively prime polynomials $a(t)$, $b(t)$ such that

$$\frac{u(t)v'(t) - u'(t)v(t) - p(t)q'(t) + p'(t)q(t)}{u^2(t) + v^2(t) + p^2(t) + q^2(t)} = \frac{a(t)b'(t) - a'(t)b(t)}{a^2(t) + b^2(t)}\,. \tag{9}$$

This can be phrased in terms of the Hopf map form (4)–(5) as requiring the existence of a complex polynomial $\mathbf{w}(t) = a(t) + \mathrm{i}\,b(t)$ such that

$$\frac{\mathrm{Im}(\overline{\boldsymbol{\alpha}}(t)\boldsymbol{\alpha}'(t) + \overline{\boldsymbol{\beta}}(t)\boldsymbol{\beta}'(t))}{|\boldsymbol{\alpha}(t)|^2 + |\boldsymbol{\beta}(t)|^2} = \frac{\mathrm{Im}(\overline{\mathbf{w}}(t)\mathbf{w}'(t))}{|\mathbf{w}(t)|^2}\,. \tag{10}$$

The left–hand side of (9) and (10) is the ERF angular velocity component in the direction of the curve tangent $\mathbf{e}_1 = \mathbf{t} = \mathbf{r}'/|\mathbf{r}'|$, and when these conditions are satisfied, a rational RMF $(\mathbf{f}_1(t), \mathbf{f}_2(t), \mathbf{f}_3(t))$ can be obtained from the ERF by a rational normal–plane rotation. Namely, we set $\mathbf{f}_1(t) = \mathbf{e}_1(t)$ and

$$\begin{bmatrix} \mathbf{f}_2(t) \\ \mathbf{f}_3(t) \end{bmatrix} = \frac{1}{a^2(t) + b^2(t)} \begin{bmatrix} a^2(t) - b^2(t) & -2\,a(t)b(t) \\ 2\,a(t)b(t) & a^2(t) - b^2(t) \end{bmatrix} \begin{bmatrix} \mathbf{e}_2(t) \\ \mathbf{e}_3(t) \end{bmatrix}. \tag{11}$$

Note that, since the determination of RMFs is an initial–value problem, one need not require coincidence of $\mathbf{f}_2, \mathbf{f}_3$ with $\mathbf{e}_2, \mathbf{e}_3$ at $t = 0$. One may, instead, impose any desired orientation of the former relative to the latter.

4 Rotation-minimizing ERFs

When $\deg(\boldsymbol{\alpha}(t), \boldsymbol{\beta}(t)) = m$ and (10) is satisfied with $\deg(\mathbf{w}(t)) = m$, we have a *Class 1* RRMF curve. The Class 1 quintics are the simplest non–degenerate RRMF curves, i.e., true space curves [5, 8]. It was observed in [12] that (10) can also be satisfied with $\deg(\mathbf{w}(t)) < m$. In particular, if (10) is satisfied with $\deg(\mathbf{w}(t)) = l < m$, we have an RRMF curve of *Class* $m - l + 1$.

Our focus here is on the case $l = 0$ (i.e., $\mathbf{w}(t) = \text{constant}$), which defines RRMF curves of Class $m+1$. For such curves, the satisfaction of (10) implies that $\mathrm{Im}(\overline{\boldsymbol{\alpha}}(t)\boldsymbol{\alpha}'(t) + \overline{\boldsymbol{\beta}}(t)\boldsymbol{\beta}'(t)) \equiv 0$. These are PH curves for which the ERF $(\mathbf{e}_1(t), \mathbf{e}_2(t), \mathbf{e}_3(t))$ is inherently rotation–minimizing, so the rational normal–plane rotation (11) is not required. Choi and Han [2] showed that the simplest non–planar curves in this category occur for $m = 3$, and characterized these Class 4 RRMF curves of degree 7 in terms of sixteen real parameters.

For given m, the RRMF curves of Class $m + 1$ (i.e., the PH curves with rotation–minimizing ERFs) have the important advantage that their rational RMFs are of lower degree than for those of Class $< m+1$. If (10) is satisfied with $\deg(\boldsymbol{\alpha}(t), \boldsymbol{\beta}(t)) = m$, we obtain an RRMF curve of degree $2m+1$ whose rational RMF vectors are of degree $4m$ when $\deg(\mathbf{w}(t)) = m$, but only degree $2m$ when $\deg(\mathbf{w}(t)) = 0$. For example, the Class 1 RRMF quintics ($m = 2$) satisfying (10) with $\deg(\mathbf{w}(t)) = 2$ have rational RMFs of degree 8, while the Class 4 RRMF curves of degree 7 ($m = 3$) satisfying (10) with $\deg(\mathbf{w}(t)) = 0$ have rational RMFs of degree 6 (both cases define true space curves).

So the degree 7 PH curves with rotation–minimizing ERFs offer rational RMFs of lower degree than the RRMF quintics studied in [5, 9]. They also offer more degrees of freedom for the design of rotation–minimizing motions. In [9] the problem of interpolating initial/final positions and orientations of a rigid body by a rational rotation–minimizing motion, defined by a Class 1 RRMF quintic, was considered. These curves nominally have sufficient free parameters to interpolate the given data, but the construction algorithm is highly non–linear in nature — the existence of interpolants was found to be contingent on a certain polynomial of degree 6 possessing a positive real root, and examples reveal that this requirement is not always satisfied.

To define a PH curve of degree 7, we use cubic complex polynomials

$$\begin{aligned} \boldsymbol{\alpha}(t) &= \boldsymbol{\alpha}_0\, b_0^3(t) + \boldsymbol{\alpha}_1\, b_1^3(t) + \boldsymbol{\alpha}_2\, b_2^3(t) + \boldsymbol{\alpha}_3\, b_3^3(t)\,, \\ \boldsymbol{\beta}(t) &= \boldsymbol{\beta}_0\, b_0^3(t) + \boldsymbol{\beta}_1\, b_1^3(t) + \boldsymbol{\beta}_2\, b_2^3(t) + \boldsymbol{\beta}_3\, b_3^3(t)\,, \end{aligned} \tag{12}$$

in (5). For these polynomials, we have

$$\begin{aligned}\mathrm{Im}(\overline{\boldsymbol{\alpha}}(t)\boldsymbol{\alpha}'(t)+\overline{\boldsymbol{\beta}}(t)\boldsymbol{\beta}'(t)) \;&=\; 3\,\mathrm{Im}(\overline{\boldsymbol{\alpha}}_0\boldsymbol{\alpha}_1+\overline{\boldsymbol{\beta}}_0\boldsymbol{\beta}_1)\,b_0^4(t)\\ &+\; \tfrac{3}{2}\,\mathrm{Im}(\overline{\boldsymbol{\alpha}}_0\boldsymbol{\alpha}_2+\overline{\boldsymbol{\beta}}_0\boldsymbol{\beta}_2)\,b_1^4(t)\\ &+\; \tfrac{1}{2}\,[\,3\,\mathrm{Im}(\overline{\boldsymbol{\alpha}}_1\boldsymbol{\alpha}_2+\overline{\boldsymbol{\beta}}_1\boldsymbol{\beta}_2)+\mathrm{Im}(\overline{\boldsymbol{\alpha}}_0\boldsymbol{\alpha}_3+\overline{\boldsymbol{\beta}}_0\boldsymbol{\beta}_3)\,]\,b_2^4(t)\\ &+\; \tfrac{3}{2}\,\mathrm{Im}(\overline{\boldsymbol{\alpha}}_1\boldsymbol{\alpha}_3+\overline{\boldsymbol{\beta}}_1\boldsymbol{\beta}_3)\,b_3^4(t)\\ &+\; 3\,\mathrm{Im}(\overline{\boldsymbol{\alpha}}_2\boldsymbol{\alpha}_3+\overline{\boldsymbol{\beta}}_2\boldsymbol{\beta}_3)\,b_4^4(t)\,, \end{aligned} \tag{13}$$

$$\begin{aligned}|\boldsymbol{\alpha}(t)|^2\pm|\boldsymbol{\beta}(t)|^2 \;&=\; (|\boldsymbol{\alpha}_0|^2\pm|\boldsymbol{\beta}_0|^2)\,b_0^6(t)\;+\;\mathrm{Re}(\overline{\boldsymbol{\alpha}}_0\boldsymbol{\alpha}_1\pm\overline{\boldsymbol{\beta}}_0\boldsymbol{\beta}_1)\,b_1^6(t)\\ &+\; [\,\tfrac{2}{5}\,\mathrm{Re}(\overline{\boldsymbol{\alpha}}_0\boldsymbol{\alpha}_2\pm\overline{\boldsymbol{\beta}}_0\boldsymbol{\beta}_2)+\tfrac{3}{5}\,(|\boldsymbol{\alpha}_1|^2\pm|\boldsymbol{\beta}_1|^2)\,]\,b_2^6(t)\\ &+\; [\,\tfrac{1}{10}\,\mathrm{Re}(\overline{\boldsymbol{\alpha}}_0\boldsymbol{\alpha}_3\pm\overline{\boldsymbol{\beta}}_0\boldsymbol{\beta}_3)+\tfrac{9}{10}\,\mathrm{Re}(\overline{\boldsymbol{\alpha}}_1\boldsymbol{\alpha}_2\pm\overline{\boldsymbol{\beta}}_1\boldsymbol{\beta}_2)\,]\,b_3^6(t)\\ &+\; [\,\tfrac{2}{5}\,\mathrm{Re}(\overline{\boldsymbol{\alpha}}_1\boldsymbol{\alpha}_3\pm\overline{\boldsymbol{\beta}}_1\boldsymbol{\beta}_3)+\tfrac{3}{5}\,(|\boldsymbol{\alpha}_2|^2\pm|\boldsymbol{\beta}_2|^2)\,]\,b_4^6(t)\\ &+\; \mathrm{Re}(\overline{\boldsymbol{\alpha}}_2\boldsymbol{\alpha}_3\pm\overline{\boldsymbol{\beta}}_2\boldsymbol{\beta}_3)\,b_5^6(t)\;+\;(|\boldsymbol{\alpha}_3|^2\pm|\boldsymbol{\beta}_3|^2)\,b_6^6(t)\,. \end{aligned} \tag{14}$$

If the curve is to have a rotation–minimizing ERF, the polynomial (13) must vanish identically, i.e., we must have

$$\begin{aligned}\mathrm{Im}(\overline{\boldsymbol{\alpha}}_0\boldsymbol{\alpha}_1+\overline{\boldsymbol{\beta}}_0\boldsymbol{\beta}_1) \;&=\; \mathrm{Im}(\overline{\boldsymbol{\alpha}}_0\boldsymbol{\alpha}_2+\overline{\boldsymbol{\beta}}_0\boldsymbol{\beta}_2) \;=\; 0\,,\\ 3\,\mathrm{Im}(\overline{\boldsymbol{\alpha}}_1\boldsymbol{\alpha}_2+\overline{\boldsymbol{\beta}}_1\boldsymbol{\beta}_2)\;+\;&\mathrm{Im}(\overline{\boldsymbol{\alpha}}_0\boldsymbol{\alpha}_3+\overline{\boldsymbol{\beta}}_0\boldsymbol{\beta}_3) \;=\; 0\,,\\ \mathrm{Im}(\overline{\boldsymbol{\alpha}}_1\boldsymbol{\alpha}_3+\overline{\boldsymbol{\beta}}_1\boldsymbol{\beta}_3) \;&=\; \mathrm{Im}(\overline{\boldsymbol{\alpha}}_2\boldsymbol{\alpha}_3+\overline{\boldsymbol{\beta}}_2\boldsymbol{\beta}_3) \;=\; 0\,. \end{aligned} \tag{15}$$

These equations impose five real constraints on the sixteen degrees of freedom in the complex coefficients $(\boldsymbol{\alpha}_i,\boldsymbol{\beta}_i)$ for $i=0,\ldots,3$. Choi and Han [2] were the first to note that certain degree 7 PH curves possess rotation–minimizing ERFs, and they described such curves in terms of sixteen real parameters.

Remark 1. For the quaternion form (3), we use a cubic polynomial

$$\mathcal{A}(t) \;=\; \mathcal{A}_0\,b_0^3(t)\;+\;\mathcal{A}_1\,b_1^3(t)\;+\;\mathcal{A}_2\,b_2^3(t)\;+\;\mathcal{A}_3\,b_3^3(t)\,. \tag{16}$$

In terms of its quaternions coefficients, the conditions (15) for a rotation–minimizing ERF become

$$\begin{aligned}\mathrm{scal}(\mathcal{A}_0\,\mathbf{i}\,\mathcal{A}_1^*) \;&=\; \mathrm{scal}(\mathcal{A}_0\,\mathbf{i}\,\mathcal{A}_2^*) \;=\; 0\,,\\ 3\,\mathrm{scal}(\mathcal{A}_1\,\mathbf{i}\,\mathcal{A}_2^*)\;+\;&\mathrm{scal}(\mathcal{A}_0\,\mathbf{i}\,\mathcal{A}_3^*) \;=\; 0\,,\\ \mathrm{scal}(\mathcal{A}_1\,\mathbf{i}\,\mathcal{A}_3^*) \;&=\; \mathrm{scal}(\mathcal{A}_2\,\mathbf{i}\,\mathcal{A}_3^*) \;=\; 0\,. \end{aligned} \tag{17}$$

Note that, when the quaternion coefficients are expressed in the scalar–vector form $\mathcal{A}_r = (a_r, \mathbf{a}_r)$, the terms in (17) are of the form

$$\mathrm{scal}(\mathcal{A}_r\,\mathbf{i}\,\mathcal{A}_s^*) \;=\; \mathbf{i}\cdot(a_r\mathbf{a}_s - a_s\mathbf{a}_r - \mathbf{a}_r\times\mathbf{a}_s)\,.$$

The conditions (15) or (17) that identify rational ERFs are equivalent to the constraints defined by equations (32)–(33) in [2].

We now derive an alternative to the characterization (15), in terms of one real and two complex constraints on the coefficients of (12). For brevity, we assume that $\mathrm{Im}(\overline{\boldsymbol{\alpha}}_0\boldsymbol{\alpha}_3) \neq 0$. This assumption is justified in Remark 2 below.

Proposition 1. *If* $\mathrm{Im}(\overline{\boldsymbol{\alpha}}_0\boldsymbol{\alpha}_3) \neq 0$*, the conditions* (15) *identifying rotation–minimizing ERFs on degree 7 PH curves are equivalent to*

$$\boldsymbol{\alpha}_1 \;=\; \frac{\mathrm{Im}(\overline{\boldsymbol{\beta}}_3\boldsymbol{\beta}_1)\,\boldsymbol{\alpha}_0 - \mathrm{Im}(\overline{\boldsymbol{\beta}}_0\boldsymbol{\beta}_1)\,\boldsymbol{\alpha}_3}{\mathrm{Im}(\overline{\boldsymbol{\alpha}}_0\boldsymbol{\alpha}_3)}\,, \tag{18}$$

$$\boldsymbol{\alpha}_2 \;=\; \frac{\mathrm{Im}(\overline{\boldsymbol{\beta}}_3\boldsymbol{\beta}_2)\,\boldsymbol{\alpha}_0 - \mathrm{Im}(\overline{\boldsymbol{\beta}}_0\boldsymbol{\beta}_2)\,\boldsymbol{\alpha}_3}{\mathrm{Im}(\overline{\boldsymbol{\alpha}}_0\boldsymbol{\alpha}_3)}\,, \tag{19}$$

$$\mathrm{Im}(\overline{\boldsymbol{\alpha}}_0\boldsymbol{\alpha}_3 + \overline{\boldsymbol{\beta}}_0\boldsymbol{\beta}_3)\;\mathrm{Im}(\overline{\boldsymbol{\alpha}}_0\boldsymbol{\alpha}_3 + 3\,\overline{\boldsymbol{\beta}}_1\boldsymbol{\beta}_2) \;=\; 0\,. \tag{20}$$

Proof : Suppose conditions (15) are satisfied with $\mathrm{Im}(\overline{\boldsymbol{\alpha}}_0\boldsymbol{\alpha}_3) \neq 0$. Setting $\boldsymbol{\alpha}_i = u_i + \mathrm{i}\,v_i$, $\boldsymbol{\beta}_i = q_i + \mathrm{i}\,p_i$ for $i = 0,\ldots,3$, the first and fourth conditions in (15) may be solved as linear equations for u_1, v_1 to obtain

$$\begin{aligned} u_1 \;&=\; \frac{(q_3p_1 - q_1p_3)u_0 - (q_0p_1 - q_1p_0)u_3}{u_0v_3 - u_3v_0}\,,\\ v_1 \;&=\; \frac{(q_3p_1 - q_1p_3)v_0 - (q_0p_1 - q_1p_0)v_3}{u_0v_3 - u_3v_0}\,, \end{aligned}$$

and since $q_3p_1 - q_1p_3 = \mathrm{Im}(\overline{\boldsymbol{\beta}}_3\boldsymbol{\beta}_1)$, $q_0p_1 - q_1p_0 = \mathrm{Im}(\overline{\boldsymbol{\beta}}_0\boldsymbol{\beta}_1)$, $u_0v_3 - u_3v_0 = \mathrm{Im}(\overline{\boldsymbol{\alpha}}_0\boldsymbol{\alpha}_3)$, we obtain expression (18) for $\boldsymbol{\alpha}_1 = u_1 + \mathrm{i}\,v_1$. Similar arguments for the second and fifth conditions in (15) yield expression (19) for $\boldsymbol{\alpha}_2 = u_2 + \mathrm{i}\,v_2$. Now from (18)–(19) we obtain

$$\mathrm{Im}(\overline{\boldsymbol{\alpha}}_1\boldsymbol{\alpha}_2) \;=\; \frac{\mathrm{Im}(\overline{\boldsymbol{\beta}}_0\boldsymbol{\beta}_1)\,\mathrm{Im}(\overline{\boldsymbol{\beta}}_3\boldsymbol{\beta}_2) - \mathrm{Im}(\overline{\boldsymbol{\beta}}_3\boldsymbol{\beta}_1)\,\mathrm{Im}(\overline{\boldsymbol{\beta}}_0\boldsymbol{\beta}_2)}{\mathrm{Im}(\overline{\boldsymbol{\alpha}}_0\boldsymbol{\alpha}_3)}\,,$$

and one can verify that the numerator of this expression simplifies to give

$$\mathrm{Im}(\overline{\boldsymbol{\alpha}}_1\boldsymbol{\alpha}_2) \;=\; \frac{\mathrm{Im}(\overline{\boldsymbol{\beta}}_0\boldsymbol{\beta}_3)\,\mathrm{Im}(\overline{\boldsymbol{\beta}}_1\boldsymbol{\beta}_2)}{\mathrm{Im}(\overline{\boldsymbol{\alpha}}_0\boldsymbol{\alpha}_3)}\,. \tag{21}$$

Substituting this into the third of equations (15) then yields condition (20), after some manipulation.

Conversely, suppose $\mathrm{Im}(\overline{\boldsymbol{\alpha}}_0\boldsymbol{\alpha}_3) \neq 0$ and conditions (18)–(20) are satisfied. Multiplying (18) and its conjugate by $\overline{\boldsymbol{\alpha}}_0$ and $\boldsymbol{\alpha}_3$ and taking the imaginary part then yields the first and fourth conditions in (15). Similarly, multiplying (19) and its conjugate by $\overline{\boldsymbol{\alpha}}_0$ and $\boldsymbol{\alpha}_3$ and taking the imaginary part gives the second and fifth conditions in (15). Finally, noting that (18)–(19) imply (21), multiplying out condition (20), substituting (21), and simplifying gives

$$\mathrm{Im}(\overline{\boldsymbol{\alpha}}_0\boldsymbol{\alpha}_3)\,[\,3\,\mathrm{Im}(\overline{\boldsymbol{\alpha}}_1\boldsymbol{\alpha}_2 + \overline{\boldsymbol{\beta}}_1\boldsymbol{\beta}_2) \;+\; \mathrm{Im}(\overline{\boldsymbol{\alpha}}_0\boldsymbol{\alpha}_3 + \overline{\boldsymbol{\beta}}_0\boldsymbol{\beta}_3)\,] \;=\; 0\,.$$

Since $\mathrm{Im}(\overline{\boldsymbol{\alpha}}_0\boldsymbol{\alpha}_3) \neq 0$ by assumption, the third condition in (15) must hold. ∎

Further simplification of the conditions (18)–(20) is achieved by adopting a special coordinate system, which proves advantageous in the context of the rotation–minimizing motion interpolation problem discussed in Section 5.

Definition 1. The PH curve specified by (5) and (12) is in *canonical form*[3] if $(\boldsymbol{\alpha}_0, \boldsymbol{\beta}_0) = w_i(1, 0)$ with $w_i \neq 0$, so that $(\mathbf{e}_1(0), \mathbf{e}_2(0), \mathbf{e}_3(0)) = (\mathbf{i}, \mathbf{j}, \mathbf{k})$.

A regular curve, with $\mathbf{r}'(0) \neq \mathbf{0}$, can always be mapped to canonical form through a spatial rotation. Since the assumption of canonical form amounts to the adoption of a particular coordinate system, any results we deduce for curves in canonical form must apply to PH curves in general position.

Lemma 1. *In canonical form with* $(\boldsymbol{\alpha}_0, \boldsymbol{\beta}_0) = w_i(1, 0)$ *the degree 7 PH curves defined by* (5) *and* (12) *that have rotation–minimizing ERFs are characterized by the conditions*

$$\boldsymbol{\alpha}_1 \;=\; \frac{\mathrm{Im}(\overline{\boldsymbol{\beta}}_3\boldsymbol{\beta}_1)}{\mathrm{Im}(\boldsymbol{\alpha}_3)}\,, \quad \boldsymbol{\alpha}_2 \;=\; \frac{\mathrm{Im}(\overline{\boldsymbol{\beta}}_3\boldsymbol{\beta}_2)}{\mathrm{Im}(\boldsymbol{\alpha}_3)}\,, \quad \mathrm{Im}(w_i\boldsymbol{\alpha}_3 + 3\,\overline{\boldsymbol{\beta}}_1\boldsymbol{\beta}_2) \;=\; 0\,. \qquad (22)$$

Proof : The expressions for $\boldsymbol{\alpha}_1, \boldsymbol{\alpha}_2$ in (22) arise on setting $(\boldsymbol{\alpha}_0, \boldsymbol{\beta}_0) = w_i(1, 0)$ in (18)–(19). Also making this substitution in (20) yields

$$w_i\,\mathrm{Im}(\boldsymbol{\alpha}_3)\;\mathrm{Im}(w_i\boldsymbol{\alpha}_3 + 3\,\overline{\boldsymbol{\beta}}_1\boldsymbol{\beta}_2) \;=\; 0\,,$$

[3]This definition of canonical form differs somewhat from prior use [5], where the initial derivative $\mathbf{r}'(0)$ was mapped to the vector $\mathbf{i}$. No scaling is invoked in Definition 1, since the parameter w_i is used to adjust $|\mathbf{r}'(0)| = w_i^2$. Instead, a standard orientation of the normal–plane vectors $\mathbf{e}_2(0)$, $\mathbf{e}_3(0)$ about the tangent $\mathbf{e}_1(0)$ is imposed in the present definition.

and since $\mathrm{Im}(\overline{\boldsymbol{\alpha}}_0\boldsymbol{\alpha}_3) = w_i\,\mathrm{Im}(\boldsymbol{\alpha}_3) \neq 0$ by assumption, we obtain the third condition in (22). ∎

Note that, since the reduction to canonical form corresponds to a spatial rotation of the hodograph, it does not affect the satisfaction of (10). We focus on canonical–form curves that satisfy (10) with $a(t)$, $b(t)$ constant, so that $\mathrm{Im}(\overline{\boldsymbol{\alpha}}\boldsymbol{\alpha}' + \overline{\boldsymbol{\beta}}\boldsymbol{\beta}') \equiv 0$. On such curves, characterized by Lemma 1, the ERF is rotation–minimizing, and the normal–plane rotation (11) is not required.

Example 1. With $w_i = 1$, the conditions (22) are satisfied by the values

$$\boldsymbol{\alpha}_0 = 1\,, \quad \boldsymbol{\alpha}_1 = -\frac{5}{3}\,, \quad \boldsymbol{\alpha}_2 = \frac{8}{3}\,, \quad \boldsymbol{\alpha}_3 = 2 + 3\,\mathrm{i}\,,$$

$$\boldsymbol{\beta}_0 = 0\,, \quad \boldsymbol{\beta}_1 = -2 - \mathrm{i}\,, \quad \boldsymbol{\beta}_2 = 3 + 2\,\mathrm{i}\,, \quad \boldsymbol{\beta}_3 = 1 - 2\,\mathrm{i}\,.$$

The cubic polynomials defining the Hopf map form of $\mathbf{r}'(t)$ are then

$$\begin{aligned} \boldsymbol{\alpha}(t) &= (1 - 8\,t + 21\,t^2 - 12\,t^3) + (3\,t^3)\,\mathrm{i}\,, \\ \boldsymbol{\beta}(t) &= (-6\,t + 21\,t^2 - 14\,t^3) + (-3\,t + 12\,t^2 - 11\,t^3)\,\mathrm{i}\,, \end{aligned}$$

and hence we find that

$$\overline{\boldsymbol{\alpha}}(t)\boldsymbol{\alpha}'(t) + \overline{\boldsymbol{\beta}}(t)\boldsymbol{\beta}'(t) = -8 + 151\,t - 1026\,t^2 + 2904\,t^3 - 3390\,t^4 + 1410\,t^5$$

is a *real* polynomial, as required for a rotation–minimizing ERF.

The components $x'(t) = |\boldsymbol{\alpha}(t)|^2 - |\boldsymbol{\beta}(t)|^2$, $y'(t) = 2\,\mathrm{Re}(\boldsymbol{\alpha}(t)\overline{\boldsymbol{\beta}}(t))$, $z'(t) = 2\,\mathrm{Im}(\boldsymbol{\alpha}(t)\overline{\boldsymbol{\beta}}(t))$ of $\mathbf{r}'(t)$ and parametric speed $\sigma(t) = |\boldsymbol{\alpha}(t)|^2 + |\boldsymbol{\beta}(t)|^2$ are

$$\begin{aligned} x'(t) &= 1 - 16\,t + 61\,t^2 - 36\,t^3 - 186\,t^4 + 348\,t^5 - 164\,t^6\,, \\ y'(t) &= -12\,t + 138\,t^2 - 616\,t^3 + 1232\,t^4 - 1020\,t^5 + 270\,t^6\,, \\ z'(t) &= 6\,t - 72\,t^2 + 340\,t^3 - 788\,t^4 + 876\,t^5 - 348\,t^6\,, \\ \sigma(t) &= 1 - 16\,t + 151\,t^2 - 684\,t^3 + 1452\,t^4 - 1356\,t^5 + 470\,t^6\,. \end{aligned}$$

One can verify that $[\,\mathbf{r}'(t) \times \mathbf{r}''(t)\,] \cdot \mathbf{r}'''(t) \not\equiv 0$, so $\mathbf{r}(t)$ is a true space curve.

Remark 2. The characterization of canonical–form degree 7 PH curves with rotation–minimizing ERFs in Proposition 1 assumed that $\mathrm{Im}(\overline{\boldsymbol{\alpha}}_0\boldsymbol{\alpha}_3) \neq 0$. In fact, this condition is necessary for a space curve. For brevity, we consider it in the case of canonical–form curves, where it becomes $\mathrm{Im}(\boldsymbol{\alpha}_3) \neq 0$. For a canonical–form curve with $\boldsymbol{\alpha}_0 = w_i \neq 0$ and $\boldsymbol{\beta}_0 = 0$, the first two conditions

in (15) become $w_i \,\mathrm{Im}(\boldsymbol{\alpha}_1) = w_i \,\mathrm{Im}(\boldsymbol{\alpha}_2) = 0$, and thus $\boldsymbol{\alpha}_0, \boldsymbol{\alpha}_1, \boldsymbol{\alpha}_2$ are all real. If we also have $\mathrm{Im}(\boldsymbol{\alpha}_3) = 0$, the remaining three conditions in (15) become

$$\mathrm{Im}(\overline{\boldsymbol{\beta}}_1 \boldsymbol{\beta}_2) \;=\; \mathrm{Im}(\overline{\boldsymbol{\beta}}_1 \boldsymbol{\beta}_3) \;=\; \mathrm{Im}(\overline{\boldsymbol{\beta}}_2 \boldsymbol{\beta}_3) \;=\; 0\,,$$

and thus $\boldsymbol{\beta}_1, \boldsymbol{\beta}_2, \boldsymbol{\beta}_3$ are of the form $\ell_1 \exp(\mathrm{i}\psi)$, $\ell_2 \exp(\mathrm{i}\psi)$, $\ell_3 \exp(\mathrm{i}\psi)$. Then, since $\boldsymbol{\alpha}(t)$ is real and $\boldsymbol{\beta}(t) = [\, \ell_1 b_1^3(t) + \ell_2 b_2^3(t) + \ell_3 b_3^3(t) \,] \exp(\mathrm{i}\psi)$, we see that $\mathbf{r}'(t)$ as defined by (5) lies in the plane through the origin with unit normal $\mathbf{n} = (0, \sin\psi, -\cos\psi)$.

5 Rotation-minimizing motion design

Choi and Han [2] considered the problem of first–order Hermite interpolation by degree 7 PH curves with rotation–minimizing ERFs, and on the basis of numerical experiments concluded that "it is highly likely that the C^1 Hermite interpolation problem is solvable for most (if not all) practical cases."

The problem considered here is a generalization of that in [2]. Instead of just initial/final points and tangents $\mathbf{p}_i, \mathbf{p}_f$ and $\mathbf{t}_i, \mathbf{t}_f$ we consider points $\mathbf{p}_i, \mathbf{p}_f$ and *frames* $(\mathbf{t}_i, \mathbf{u}_i, \mathbf{v}_i)$ and $(\mathbf{t}_f, \mathbf{u}_f, \mathbf{v}_f)$ specifying the initial/final positions and *orientations* of a rigid body that is to execute a rotation–minimizing motion. As noted above, this problem has already been considered [9] in the context of Class 1 RRMF quintics, but with these curves it was not possible to ensure the existence of interpolants for arbitrary spatial motion data. Furthermore, when interpolants exist, there are no residual degrees of freedom to improve shape quality. This is a significant concern since — as observed in [9] — the interpolation of end points and frames by rotation–minimizing motions does not necessarily yield trajectories of good shape quality.

Remark 3. In the interpolation of C^1 Hermite data with PH quintics [7], free parameters ϕ_0, ϕ_1, ϕ_2 associated with the quaternion coefficients arise. Since the shape of the curve depends only their differences, it is customary to take $\phi_1 = 0$. In the present context, however, this assumption is not appropriate since it alters the ERF orientation. On proceeding to degree 7 PH curves, four additional parameters are introduced through another quaternion coefficient, and two more in relaxing from C^1 to G^1 data. Together with ϕ_0, ϕ_1, ϕ_2 this gives a total of nine freedoms, of which five are used to satisfy the conditions (22) for a rotation–minimizing ERF, and two are employed to interpolate the orientations of $(\mathbf{u}_i, \mathbf{v}_i)$ and $(\mathbf{u}_f, \mathbf{v}_f)$ about $\mathbf{t}_i$ and $\mathbf{t}_f$. Hence, the interpolation problem addressed here incorporates two free parameters.

Henceforth, we assume that $\mathbf{p}_i = (0,0,0)$ and $(\mathbf{t}_i, \mathbf{u}_i, \mathbf{v}_i) = (\mathbf{i}, \mathbf{j}, \mathbf{k})$. Since integrating the hodograph (5) introduces a free constant $\mathbf{r}(0) = \mathbf{p}_i$, the former choice involves no loss of generality. The latter is achieved through a spatial rotation R that transforms[4] the curve to canonical form (see Section 4). The rotation R must also be applied to the vectors $(\mathbf{t}_f, \mathbf{u}_f, \mathbf{v}_f)$ and $\Delta\mathbf{p} = \mathbf{p}_f - \mathbf{p}_i$. Once the interpolation problem is solved for this standard configuration, the inverse rotation R^{-1} can be applied to restore the solution to general position. In standard configuration, the remaining interpolation requirements are:

(a) matching $\mathbf{e}_1(1)$ to the specified end–tangent $\mathbf{t}_f$;

(b) matching $\mathbf{e}_2(1), \mathbf{e}_3(1)$ to the the normal–plane vectors $\mathbf{u}_f, \mathbf{v}_f$;

(c) matching $\mathbf{r}(1) - \mathbf{r}(0)$ to the displacement $\Delta\mathbf{p} = \mathbf{p}_f - \mathbf{p}_i$.

5.1 Interpolation of tangent

The interpolation condition (a) corresponds to the requirement that

$$\mathbf{e}_1(1) \;=\; \frac{(|\boldsymbol{\alpha}_3|^2 - |\boldsymbol{\beta}_3|^2,\, 2\,\mathrm{Re}(\boldsymbol{\alpha}_3\overline{\boldsymbol{\beta}}_3),\, 2\,\mathrm{Im}(\boldsymbol{\alpha}_3\overline{\boldsymbol{\beta}}_3))}{|\boldsymbol{\alpha}_3|^2 + |\boldsymbol{\beta}_3|^2} \;=\; \mathbf{t}_f\,.$$

Writing $\mathbf{t}_f = (\lambda, \mu, \nu)$ where $\lambda^2 + \mu^2 + \nu^2 = 1$, and defining ϕ by

$$\mu + \mathrm{i}\,\nu \;=\; \sqrt{1-\lambda^2}\,\exp(\mathrm{i}\phi)\,, \tag{23}$$

this is equivalent to

$$\frac{|\boldsymbol{\alpha}_3|^2 - |\boldsymbol{\beta}_3|^2}{|\boldsymbol{\alpha}_3|^2 + |\boldsymbol{\beta}_3|^2} \;=\; \lambda\,, \qquad \frac{2\,\boldsymbol{\alpha}_3\overline{\boldsymbol{\beta}}_3}{|\boldsymbol{\alpha}_3|^2 + |\boldsymbol{\beta}_3|^2} \;=\; \sqrt{1-\lambda^2}\,\exp(\mathrm{i}\phi)\,. \tag{24}$$

The solutions to (24) can be expressed in terms of parameters w_f and θ as

$$\boldsymbol{\alpha}_3 \;=\; w_f\,\sqrt{\tfrac{1}{2}(1+\lambda)}\;\exp(\mathrm{i}(\phi + \tfrac{1}{2}\theta))\,, \quad \boldsymbol{\beta}_3 \;=\; w_f\,\sqrt{\tfrac{1}{2}(1-\lambda)}\;\exp(\mathrm{i}\tfrac{1}{2}\theta)\,. \tag{25}$$

Condition (a) is satisfied by choosing $\boldsymbol{\alpha}_3, \boldsymbol{\beta}_3$ of the form (25). Note that, since $|\mathbf{r}'(1)| = w_f^2$, the parameter w_f controls the mangitude of the final derivative.

[4]This is most easily realized as a sequence of two rotations — the first being a rotation that maps $\mathbf{t}_i$ onto $\mathbf{i}$, and the second being a rotation about $\mathbf{i}$ that maps $\mathbf{u}_i$, $\mathbf{v}_i$ onto $\mathbf{j}$, $\mathbf{k}$.

5.2 Interpolation of normal-plane vectors

The satisfaction of condition (b) is facilitated by the following result.

Lemma 2. *Consider the orthonormal frame* $(\mathbf{e}_1, \mathbf{e}_2, \mathbf{e}_3)$ *defined in terms of a given quaternion* $\mathcal{A} = u + v\,\mathbf{i} + p\,\mathbf{j} + q\,\mathbf{k}$ *by*

$$\mathbf{e}_1 \,=\, \frac{\mathcal{A}\,\mathbf{i}\,\mathcal{A}^*}{|\mathcal{A}|^2}\,, \quad \mathbf{e}_2 \,=\, \frac{\mathcal{A}\,\mathbf{j}\,\mathcal{A}^*}{|\mathcal{A}|^2}\,, \quad \mathbf{e}_3 \,=\, \frac{\mathcal{A}\,\mathbf{k}\,\mathcal{A}^*}{|\mathcal{A}|^2}\,.$$

Then, under the transformation

$$\mathcal{A} \,\to\, \mathcal{A}\,\mathcal{Q}\,, \quad \mathcal{Q} \,=\, \cos\tfrac{1}{2}\theta + \sin\tfrac{1}{2}\theta\,\mathbf{i}\,, \tag{26}$$

this frame transforms according to

$$(\mathbf{e}_1, \mathbf{e}_2, \mathbf{e}_3) \,\to\, (\mathbf{e}_1, \cos\theta\,\mathbf{e}_2 + \sin\theta\,\mathbf{e}_3, -\sin\theta\,\mathbf{e}_2 + \cos\theta\,\mathbf{e}_3)\,. \tag{27}$$

In other words, $\mathbf{e}_1$ *is unaltered but* $\mathbf{e}_2, \mathbf{e}_3$ *rotate through angle* θ *about* $\mathbf{e}_1$*.*

Proof : The transformation rule (27) follows directly from the fact that the quaternion $\mathcal{Q}$ defined by (26) satisfies $\mathcal{Q}\,\mathbf{i}\,\mathcal{Q}^* = \mathbf{i}$ and

$$\mathcal{Q}\,\mathbf{j}\,\mathcal{Q}^* \,=\, \cos\theta\,\mathbf{j} \,+\, \sin\theta\,\mathbf{k}\,, \quad \mathcal{Q}\,\mathbf{k}\,\mathcal{Q}^* \,=\, -\,\sin\theta\,\mathbf{j} \,+\, \cos\theta\,\mathbf{k}\,. \quad \blacksquare$$

Writing $\mathcal{A} = \boldsymbol{\alpha} + \mathbf{k}\,\boldsymbol{\beta}$ for appropriate complex numbers $\boldsymbol{\alpha}$, $\boldsymbol{\beta}$ we see that for the Hopf map form, the equivalent frame

$$\begin{aligned}
\mathbf{e}_1 \,&=\, \frac{\big(\,|\boldsymbol{\alpha}|^2 - |\boldsymbol{\beta}|^2, 2\,\mathrm{Re}\,(\boldsymbol{\alpha}\overline{\boldsymbol{\beta}}), 2\,\mathrm{Im}\,(\boldsymbol{\alpha}\overline{\boldsymbol{\beta}})\,\big)}{|\boldsymbol{\alpha}|^2 + |\boldsymbol{\beta}|^2}\,, \\
\mathbf{e}_2 \,&=\, \frac{\big(-2\,\mathrm{Re}\,(\boldsymbol{\alpha}\boldsymbol{\beta}), \mathrm{Re}\,(\boldsymbol{\alpha}^2 - \boldsymbol{\beta}^2), \mathrm{Im}\,(\boldsymbol{\alpha}^2 + \boldsymbol{\beta}^2)\,\big)}{|\boldsymbol{\alpha}|^2 + |\boldsymbol{\beta}|^2}\,, \\
\mathbf{e}_3 \,&=\, \frac{\big(\,2\,\mathrm{Im}\,(\boldsymbol{\alpha}\boldsymbol{\beta}), -\,\mathrm{Im}\,(\boldsymbol{\alpha}^2 - \boldsymbol{\beta}^2), \mathrm{Re}\,(\boldsymbol{\alpha}^2 + \boldsymbol{\beta}^2)\,\big)}{|\boldsymbol{\alpha}|^2 + |\boldsymbol{\beta}|^2}\,,
\end{aligned} \tag{28}$$

also obeys (27) under the corresponding transformation

$$(\boldsymbol{\alpha}, \boldsymbol{\beta}) \,\to\, (\boldsymbol{\alpha}\exp(\mathrm{i}\tfrac{1}{2}\theta), \boldsymbol{\beta}\exp(\mathrm{i}\tfrac{1}{2}\theta))\,.$$

Lemma 2 allows one to enforce any desired orientation of the ERF normal–plane vectors $\mathbf{e}_2(t), \mathbf{e}_3(t)$ about the tangent $\mathbf{e}_1(t)$ at a particular point t on a

spatial PH curve $\mathbf{r}(t)$. This property will be used to match the ERF at $t = 1$ to the prescribed final frame $(\mathbf{t}_f, \mathbf{u}_f, \mathbf{v}_f)$. Now let

$$\begin{aligned}
\hat{\mathbf{e}}_1 &= \lambda\,\mathbf{i} + \sqrt{1-\lambda^2}\,\cos\phi\,\mathbf{j} + \sqrt{1-\lambda^2}\,\sin\phi\,\mathbf{k}\,,\\
\hat{\mathbf{e}}_2 &= -\sqrt{1-\lambda^2}\,\cos\phi\,\mathbf{i} + (\lambda\cos^2\phi - \sin^2\phi)\,\mathbf{j} + (1+\lambda)\cos\phi\,\sin\phi\,\mathbf{k}\,,\\
\hat{\mathbf{e}}_3 &= \sqrt{1-\lambda^2}\,\sin\phi\,\mathbf{i} - (1+\lambda)\cos\phi\,\sin\phi\,\mathbf{j} + (\cos^2\phi - \lambda\sin^2\phi)\,\mathbf{k}\,,
\end{aligned}$$

be the frame defined by substituting (25) with $\theta = 0$ for $\boldsymbol{\alpha}, \boldsymbol{\beta}$ in (28). Then the value of θ that matches the final ERF vectors $\mathbf{e}_2(1)$, $\mathbf{e}_3(1)$ to $\mathbf{u}_f$, $\mathbf{v}_f$ is determined by the conditions

$$\cos\theta\,\hat{\mathbf{e}}_2 + \sin\theta\,\hat{\mathbf{e}}_3 = \mathbf{u}_f\,, \qquad -\sin\theta\,\hat{\mathbf{e}}_2 + \cos\theta\,\hat{\mathbf{e}}_3 = \mathbf{v}_f\,,$$

from which we may deduce that

$$(\cos\theta, \sin\theta) = (\hat{\mathbf{e}}_2\cdot\mathbf{u}_f, \hat{\mathbf{e}}_3\cdot\mathbf{u}_f) = (\hat{\mathbf{e}}_3\cdot\mathbf{v}_f, -\hat{\mathbf{e}}_2\cdot\mathbf{v}_f)\,. \tag{29}$$

Condition (b) is satisfied by using in (25) the θ value defined by (29).

5.3 Interpolation of end-point displacement

Satisfaction of condition (c) is equivalent to

$$\mathbf{r}(1) - \mathbf{r}(0) = \int_0^1 \mathbf{r}'(t)\,\mathrm{d}t = \Delta\mathbf{p}\,, \tag{30}$$

where $\Delta\mathbf{p} = \mathbf{p}_f - \mathbf{p}_i = (\Delta x, \Delta y, \Delta z)$. Using the Hopf map form (5), we have

$$\int_0^1 |\boldsymbol{\alpha}(t)|^2 - |\boldsymbol{\beta}(t)|^2\,\mathrm{d}t = \Delta x\,, \qquad \int_0^1 2\,\boldsymbol{\alpha}(t)\overline{\boldsymbol{\beta}}(t)\,\mathrm{d}t = \Delta y + \mathrm{i}\,\Delta z\,. \tag{31}$$

We now take stock of the available freedoms. In canonical form $\boldsymbol{\alpha}_0, \boldsymbol{\beta}_0$ depend only on the parameter w_i. Moreover, interpolation of $(\mathbf{t}_f, \mathbf{u}_f, \mathbf{v}_f)$ implies that $\boldsymbol{\alpha}_3, \boldsymbol{\beta}_3$ are specified by (25), where θ is defined by (29), and thus depend only on w_f. Now by Lemma 1, the coefficients of the cubics (12) must satisfy the conditions (22) if the curve is to possess a rotation–minimizing ERF. The first two conditions specify $\boldsymbol{\alpha}_1, \boldsymbol{\alpha}_2$ in terms of $\boldsymbol{\beta}_1, \boldsymbol{\beta}_2$ and $\boldsymbol{\alpha}_3, \boldsymbol{\beta}_3$. Thus, only w_i, w_f and $\boldsymbol{\beta}_1, \boldsymbol{\beta}_2$ remain as free variables, incorporating six scalar degrees of freedom, while four scalar constraints remain to be satisfied — namely, the third of conditions (22) and the displacement interpolation (31).

Hence, the motion interpolation problem embodies two residual freedoms. In the approach described below w_i and w_f are regarded as free parameters, that appear in a system of four equations for the real and imaginary parts of $\boldsymbol{\beta}_1$, $\boldsymbol{\beta}_2$. Since $|\mathbf{r}'(0)| = w_i^2$ and $|\mathbf{r}'(1)| = w_f^2$, varying these parameters offers a natural means to manipulate the shape of the trajectory, while preserving interpolation of the end points/orientations. Henceforth, for brevity, we write

$$c \;=\; \cos(\phi + \tfrac{1}{2}\theta)\,, \quad s \;=\; \sin(\phi + \tfrac{1}{2}\theta)\,, \tag{32}$$

$$k \;=\; \sqrt{\tfrac{1}{2}(1+\lambda)}\,, \quad l \;=\; \sqrt{\tfrac{1}{2}(1-\lambda)}\,, \quad m \;=\; \frac{l}{k}\frac{1}{s}\,. \tag{33}$$

These are known values, once the end frames have been interpolated. Thus, setting $\boldsymbol{\beta}_1 = \mathbf{z}_1 \exp(\mathrm{i}\tfrac{1}{2}\theta)$, $\boldsymbol{\beta}_2 = \mathbf{z}_2 \exp(\mathrm{i}\tfrac{1}{2}\theta)$ with $\mathbf{z}_1 = x_1 + \mathrm{i}\, y_1$, $\mathbf{z}_2 = x_2 + \mathrm{i}\, y_2$ and using (22) and (25) — with θ defined by (29) — the coefficients of the cubics (12) become

$$(\boldsymbol{\alpha}_0, \boldsymbol{\alpha}_1, \boldsymbol{\alpha}_2, \boldsymbol{\alpha}_3) \;=\; (w_i, m\, y_1, m\, y_2, w_f k(c + \mathrm{i}\, s))\,, \tag{34}$$

$$(\boldsymbol{\beta}_0, \boldsymbol{\beta}_1, \boldsymbol{\beta}_2, \boldsymbol{\beta}_3) \;=\; (0, \mathbf{z}_1 \exp(\mathrm{i}\tfrac{1}{2}\theta), \mathbf{z}_2 \exp(\mathrm{i}\tfrac{1}{2}\theta), w_f l \exp(\mathrm{i}\tfrac{1}{2}\theta))\,, \tag{35}$$

and they must also satisfy the third condition in (22). Recall from Remark 2 that we require $\mathrm{Im}(\boldsymbol{\alpha}_3) \neq 0$ for a space curve. Since $w_f \neq 0$ for a regular curve, this implies that $ks \neq 0$. Hence, the quantity m in (33) is finite.

Now for the cubics (12), the first integrand in (31) is given by (14) with the minus sign, while the second integrand is

$$\begin{aligned}
2\,\boldsymbol{\alpha}(t)\overline{\boldsymbol{\beta}}(t) \;=\;& 2\,\boldsymbol{\alpha}_0\overline{\boldsymbol{\beta}}_0\, b_0^6(t) \;+\; (\boldsymbol{\alpha}_0\overline{\boldsymbol{\beta}}_1 + \boldsymbol{\alpha}_1\overline{\boldsymbol{\beta}}_0)\, b_1^6(t) \\
&+\; \tfrac{2}{5}\,(\boldsymbol{\alpha}_0\overline{\boldsymbol{\beta}}_2 + \boldsymbol{\alpha}_2\overline{\boldsymbol{\beta}}_0 + 3\,\boldsymbol{\alpha}_1\overline{\boldsymbol{\beta}}_1)\, b_2^6(t) \\
&+\; \tfrac{1}{10}\,[\,\boldsymbol{\alpha}_0\overline{\boldsymbol{\beta}}_3 + \boldsymbol{\alpha}_3\overline{\boldsymbol{\beta}}_0 + 9\,(\boldsymbol{\alpha}_1\overline{\boldsymbol{\beta}}_2 + \boldsymbol{\alpha}_2\overline{\boldsymbol{\beta}}_1)\,]\, b_3^6(t) \\
&+\; \tfrac{2}{5}\,(\boldsymbol{\alpha}_1\overline{\boldsymbol{\beta}}_3 + \boldsymbol{\alpha}_3\overline{\boldsymbol{\beta}}_1 \;+\; 3\,\boldsymbol{\alpha}_2\overline{\boldsymbol{\beta}}_2)\, b_4^6(t) \\
&+\; (\boldsymbol{\alpha}_2\overline{\boldsymbol{\beta}}_3 + \boldsymbol{\alpha}_3\overline{\boldsymbol{\beta}}_2)\, b_5^6(t) \;+\; 2\,\boldsymbol{\alpha}_3\overline{\boldsymbol{\beta}}_3\, b_6^6(t)\,.
\end{aligned}$$

Since the definite integral of a Bernstein–form polynomial of degree n is just the sum of its coefficients divided by $n+1$, conditions (31) can be written as

$$\begin{aligned}
&10(|\boldsymbol{\alpha}_0|^2 - |\boldsymbol{\beta}_0|^2) \;+\; 10\,\mathrm{Re}(\overline{\boldsymbol{\alpha}}_0\boldsymbol{\alpha}_1 - \overline{\boldsymbol{\beta}}_0\boldsymbol{\beta}_1) \\
&+\; 4\,\mathrm{Re}(\overline{\boldsymbol{\alpha}}_0\boldsymbol{\alpha}_2 - \overline{\boldsymbol{\beta}}_0\boldsymbol{\beta}_2) + 6\,(|\boldsymbol{\alpha}_1|^2 - |\boldsymbol{\beta}_1|^2) \\
&+\; \mathrm{Re}(\overline{\boldsymbol{\alpha}}_0\boldsymbol{\alpha}_3 - \overline{\boldsymbol{\beta}}_0\boldsymbol{\beta}_3) + 9\,\mathrm{Re}(\overline{\boldsymbol{\alpha}}_1\boldsymbol{\alpha}_2 - \overline{\boldsymbol{\beta}}_1\boldsymbol{\beta}_2) \\
&+\; 4\,\mathrm{Re}(\overline{\boldsymbol{\alpha}}_1\boldsymbol{\alpha}_3 - \overline{\boldsymbol{\beta}}_1\boldsymbol{\beta}_3) + 6\,(|\boldsymbol{\alpha}_2|^2 - |\boldsymbol{\beta}_2|^2) \\
&+\; 10\,\mathrm{Re}(\overline{\boldsymbol{\alpha}}_2\boldsymbol{\alpha}_3 - \overline{\boldsymbol{\beta}}_2\boldsymbol{\beta}_3) \;+\; 10(|\boldsymbol{\alpha}_3|^2 - |\boldsymbol{\beta}_3|^2) \;=\; 70\,\Delta x\,,
\end{aligned} \tag{36}$$

$$
\begin{aligned}
&20\,\boldsymbol{\alpha}_0\overline{\boldsymbol{\beta}}_0 \,+\, 10(\boldsymbol{\alpha}_0\overline{\boldsymbol{\beta}}_1 + \boldsymbol{\alpha}_1\overline{\boldsymbol{\beta}}_0)\\
&+\, 4(\boldsymbol{\alpha}_0\overline{\boldsymbol{\beta}}_2 + \boldsymbol{\alpha}_2\overline{\boldsymbol{\beta}}_0) + 12\,\boldsymbol{\alpha}_1\overline{\boldsymbol{\beta}}_1\\
&+\, \boldsymbol{\alpha}_0\overline{\boldsymbol{\beta}}_3 + \boldsymbol{\alpha}_3\overline{\boldsymbol{\beta}}_0 + 9\,(\boldsymbol{\alpha}_1\overline{\boldsymbol{\beta}}_2 + \boldsymbol{\alpha}_2\overline{\boldsymbol{\beta}}_1)\\
&+\, 4(\boldsymbol{\alpha}_1\overline{\boldsymbol{\beta}}_3 + \boldsymbol{\alpha}_3\overline{\boldsymbol{\beta}}_1) \,+\, 12\,\boldsymbol{\alpha}_2\overline{\boldsymbol{\beta}}_2\\
&+\, 10(\boldsymbol{\alpha}_2\overline{\boldsymbol{\beta}}_3 + \boldsymbol{\alpha}_3\overline{\boldsymbol{\beta}}_2) \,+\, 20\,\boldsymbol{\alpha}_3\overline{\boldsymbol{\beta}}_3 \,=\, 70\,(\Delta y + \mathrm{i}\,\Delta z)\,. \qquad (37)
\end{aligned}
$$

We substitute from (34)–(35) into the third of equations (22) and equation (36). In equation (37), we multiply both sides by $\exp(\mathrm{i}\frac{1}{2}\theta)$, substitute (34)–(35), and separate real and imaginary parts. This yields the following system of four quadratic equations

$$
f_1(x_1, y_1, x_2, y_2) \,=\, k\,w_i w_f\,s \,+\, 3(x_1y_2 - x_2y_1) \,=\, 0\,, \qquad (38)
$$

$$
\begin{aligned}
f_2(x_1, y_1, x_2, y_2) \,&=\, 10\,w_i^2 \,+\, m\,w_i(10y_1 + 4y_2) \,+\, 6m^2(y_1^2 + y_2^2)\\
&+\, 9m^2y_1y_2 \,-\, 6(x_1^2 + y_1^2 + x_2^2 + y_2^2) \,-\, 9(x_1x_2 + y_1y_2) \,+\, k\,w_i w_f\,c\\
&-\, km\,w_f\,[\,4(sx_1 - cy_1) + 10(sx_2 - cy_2)\,] \,+\, 10\,w_f^2\,\lambda \,-\, 70\,\Delta x \,=\, 0\,, \qquad (39)
\end{aligned}
$$

$$
\begin{aligned}
f_3(x_1, y_1, x_2, y_2) \,&=\, w_i(10x_1 + 4x_2) \,+\, 9m(x_1y_2 + x_2y_1) \,+\, 12m(x_1y_1 + x_2y_2)\\
&+\, l\,w_i w_f \,+\, lm\,w_f(4y_1 + 10y_2) \,+\, k\,w_f\,[\,4(cx_1 + sy_1) + 10(cx_2 + sy_2)\,]\\
&+\, 20\,kl\,w_f^2 c \,-\, 70\,(\cos\tfrac{1}{2}\theta\,\Delta y - \sin\tfrac{1}{2}\theta\,\Delta z) \,=\, 0\,, \qquad (40)
\end{aligned}
$$

$$
\begin{aligned}
f_4(x_1, y_1, x_2, y_2) \,&=\, -\,w_i(10y_1 + 4y_2) \,-\, m\,(12y_1^2 + 18y_1y_2 + 12y_2^2)\\
&+\, k\,w_f\,[\,4(sx_1 - cy_1) + 10(sx_2 - cy_2)\,] \,+\, 20\,kl\,w_f^2 s\\
&-\, 70\,(\sin\tfrac{1}{2}\theta\,\Delta y + \cos\tfrac{1}{2}\theta\,\Delta z) \,=\, 0\,, \qquad (41)
\end{aligned}
$$

in the four real variables x_1, y_1, x_2, y_2, where $\lambda, \phi, \Delta x, \Delta y, \Delta z$ and (32)–(33) are known quantities, while w_i, w_f are parameters that can be used to vary the end–derivative magnitudes, since $|\mathbf{r}'(0)| = w_i^2$ and $|\mathbf{r}'(1)| = w_f^2$.

Remark 4. Apart from the terms involving $\Delta x, \Delta y, \Delta z$ equations (38)–(41) are quadratic in $w_i, w_f, x_1, y_1, x_2, y_2$. Hence, if (x_1, x_2, y_1, y_2) is a solution for parameter values (w_i, w_f) when $|\Delta\mathbf{p}| = 1$, then $\sqrt{L}(x_1, x_2, y_1, y_2)$ is a solution for the parameter values $\sqrt{L}(w_i, w_f)$ when $|\Delta\mathbf{p}| = L$. So equations (38)–(41) can be solved, without loss of generality, under the assumption that $|\Delta\mathbf{p}| = 1$, and an appropriate scaling can be applied *a posteriori* to the solution.

From Remark 4, we observe that canonical–form input data depends upon only five essential parameters — namely, two to specify the direction of $\Delta\mathbf{p}$, and three to determine the orientation of the end–frame $(\mathbf{t}_f, \mathbf{u}_f, \mathbf{v}_f)$.

Once solutions x_1, y_1, x_2, y_2 to the system (38)–(41) have been computed, we may determine the complex coefficients (34)–(35), where $\mathbf{z}_1 = x_1 + \mathrm{i}\, y_1$ and $\mathbf{z}_2 = x_2 + \mathrm{i}\, y_2$. The corresponding quaternion coefficients are $\mathcal{A}_i = \boldsymbol{\alpha}_i + \mathbf{k}\,\boldsymbol{\beta}_i$ for $i = 0, \ldots, 3$. Then, substituting (16) into (3) and integrating yields the Bézier form of a degree 7 PH curve,

$$\mathbf{r}(t) \;=\; \sum_{i=0}^{7} \mathbf{p}_i \, b_i^7(t)\,,$$

with control points $\mathbf{p}_0, \ldots, \mathbf{p}_7$ given by

$$\begin{aligned}
\mathbf{p}_1 &= \mathbf{p}_0 + \frac{1}{7}\,\mathcal{A}_0\,\mathbf{i}\,\mathcal{A}_0^*\,,\\
\mathbf{p}_2 &= \mathbf{p}_1 + \frac{1}{14}(\mathcal{A}_0\,\mathbf{i}\,\mathcal{A}_1^* + \mathcal{A}_1\,\mathbf{i}\,\mathcal{A}_0^*)\,,\\
\mathbf{p}_3 &= \mathbf{p}_2 + \frac{1}{35}(\mathcal{A}_0\,\mathbf{i}\,\mathcal{A}_2^* + 3\,\mathcal{A}_1\,\mathbf{i}\,\mathcal{A}_1^* + \mathcal{A}_2\,\mathbf{i}\,\mathcal{A}_0^*)\,,\\
\mathbf{p}_4 &= \mathbf{p}_3 + \frac{1}{140}(\mathcal{A}_0\,\mathbf{i}\,\mathcal{A}_3^* + \mathcal{A}_3\,\mathbf{i}\,\mathcal{A}_0^* + 9\mathcal{A}_1\,\mathbf{i}\,\mathcal{A}_2^* + 9\mathcal{A}_2\,\mathbf{i}\,\mathcal{A}_1^*)\,,\\
\mathbf{p}_5 &= \mathbf{p}_4 + \frac{1}{35}(\mathcal{A}_1\,\mathbf{i}\,\mathcal{A}_3^* + 3\,\mathcal{A}_2\,\mathbf{i}\,\mathcal{A}_2^* + \mathcal{A}_3\,\mathbf{i}\,\mathcal{A}_1^*)\,,\\
\mathbf{p}_6 &= \mathbf{p}_5 + \frac{1}{14}(\mathcal{A}_2\,\mathbf{i}\,\mathcal{A}_3^* + \mathcal{A}_3\,\mathbf{i}\,\mathcal{A}_2^*)\,,\\
\mathbf{p}_7 &= \mathbf{p}_6 + \frac{1}{7}\,\mathcal{A}_3\,\mathbf{i}\,\mathcal{A}_3^*\,,
\end{aligned} \tag{42}$$

where we set $\mathbf{p}_0 = \mathbf{p}_i$. By construction, this curve has a rotation–minimizing ERF, with initial and final instances that coincide (in standard configuration) with the specified frames $(\mathbf{t}_i, \mathbf{u}_i, \mathbf{v}_i)$ and $(\mathbf{t}_f, \mathbf{u}_f, \mathbf{v}_f)$. Also, $\mathbf{p}_7 - \mathbf{p}_0$ coincides with the specified displacement vector $\Delta\mathbf{p} = (\Delta x, \Delta y, \Delta z) = \mathbf{p}_f - \mathbf{p}_i$.

5.4 Motion interpolation algorithm

The following algorithm summarizes the procedure for constructing a rigid–body motion, described by a degree 7 PH curve with a rotation–minimizing Euler–Rodrigues frame, that matches initial/final positions and orientations.

Algorithm

input: initial/final points $\mathbf{p}_i$, $\mathbf{p}_f$ and frames $(\mathbf{t}_i, \mathbf{u}_i, \mathbf{v}_i)$, $(\mathbf{t}_f, \mathbf{u}_f, \mathbf{v}_f)$

1. identify the spatial rotation R that maps the initial frame $(\mathbf{t}_i, \mathbf{u}_i, \mathbf{v}_i)$ onto $(\mathbf{i}, \mathbf{j}, \mathbf{k})$ and apply it also to the final frame $(\mathbf{t}_f, \mathbf{u}_f, \mathbf{v}_f)$ and the displacement vector $\Delta\mathbf{p} = \mathbf{p}_f - \mathbf{p}_i$;

2. determine ϕ from the components (λ, μ, ν) of $\mathbf{t}_f$ using (23);

3. find the θ value that matches $\mathbf{e}_2(1)$, $\mathbf{e}_3(1)$ to $\mathbf{u}_f$, $\mathbf{v}_f$ from (29);

4. compute the constants specified by expressions (32)–(33);

5. choose values for w_i, w_f appropriate to the desired magnitudes of the end derivatives;

6. identify a real solution (x_1, y_1, x_2, y_2) of the system (38)–(41);

7. with $\mathbf{z}_1 = x_1 + \mathrm{i}\, y_1$ and $\mathbf{z}_2 = x_2 + \mathrm{i}\, y_2$ determine $(\boldsymbol{\alpha}_r, \boldsymbol{\beta}_r)$ for $r = 0, \ldots, 3$ from expressions (34)–(35);

8. compute the corresponding quaternion coefficients $\mathcal{A}_r = \boldsymbol{\alpha}_r + \mathbf{k}\,\boldsymbol{\beta}_r$ for $r = 0, \ldots, 3$ and the Bézier control points $\mathbf{p}_0, \ldots, \mathbf{p}_7$ of the curve $\mathbf{r}(t)$ from (42);

9. compute the rotation–minimizing ERF using (8);

10. apply the inverse R^{-1} of the spatial rotation used in step 1, to restore the curve $\mathbf{r}(t)$ to its original orientation.

output: degree 7 PH curve $\mathbf{r}(t)$ with rotation–minimizing ERF $(\mathbf{e}_1(t), \mathbf{e}_2(t), \mathbf{e}_3(t))$ where $\mathbf{r}(0) = \mathbf{p}_i$, $(\mathbf{e}_1(0), \mathbf{e}_2(0), \mathbf{e}_3(0)) = (\mathbf{t}_i, \mathbf{u}_i, \mathbf{v}_i)$ and $\mathbf{r}(1) = \mathbf{p}_f$, $(\mathbf{e}_1(1), \mathbf{e}_2(1), \mathbf{e}_3(1)) = (\mathbf{t}_f, \mathbf{u}_f, \mathbf{v}_f)$.

6 Computed examples

The system (38)–(41), in which w_i and w_f are free parameters, imposes four quadratic constraints on the real variables x_1, y_1, x_2, y_2. Experiments indicate that, for appropriately chosen w_i, w_f values, this system is well–conditioned, and numerical methods for its solution converge rapidly to machine precision. Since the parameters w_i and w_f are found to strongly influence the existence and shape properties of the solutions, their values should be determined by consideration of suitable shape measures, rather than *ad hoc* choice.

6.1 Integral shape measures

In the Hopf map form, the curvature of the PH curve specified by (4)–(5) can be expressed [10] as

$$\kappa(t) \;=\; 2\,\frac{|\,\boldsymbol{\alpha}(t)\boldsymbol{\beta}'(t) - \boldsymbol{\alpha}'(t)\boldsymbol{\beta}(t)\,|}{\sigma^2(t)}\,, \tag{43}$$

where $\sigma(t) = |\boldsymbol{\alpha}(t)|^2 + |\boldsymbol{\beta}(t)|^2$. Hence, the shape measures defined by

$$I_m \;=\; \int_0^1 \kappa^m(t)\,\sigma(t)\;\mathrm{d}t\,, \qquad m = 0, 1, 2$$

can, in principle, be evaluated by factorizing $\sigma(t)$ and performing a partial fraction expansion of the integrand. The simplest shape measure is the total arc length,

$$S \;=\; I_0 \;=\; \int_0^1 \sigma(t)\;\mathrm{d}t \;=\; \int_0^1 |\boldsymbol{\alpha}(t)|^2 + |\boldsymbol{\beta}(t)|^2\;\mathrm{d}t\,. \tag{44}$$

By arguments analogous to those used in Section 5, one can verify that the dependence of S on x_1, y_1, x_2, y_2 and the parameters w_i, w_f is defined by

$$\begin{aligned} 70\,S(x_1, y_1, x_2, y_2) \;=\; & 10\,w_i^2 \;+\; m\,w_i(10y_1 + 4y_2) \;+\; 6m^2(y_1^2 + y_2^2) \\ & + 9m^2 y_1 y_2 \;+\; 6(x_1^2 + y_1^2 + x_2^2 + y_2^2) \;+\; 9(x_1 x_2 + y_1 y_2) \;+\; k\,w_i w_f\,c \\ & + km\,w_f\,[\,4(sx_1 + cy_1) + 10(sx_2 + cy_2)\,] \;+\; 10\,w_f^2\,. \end{aligned} \tag{45}$$

The integral I_1, which may be regarded as a measure of the "total turning" of the curve tangent, is less commonly used in practice. Finally, the $m = 2$ case corresponds to the *elastic bending energy*,

$$E \;=\; I_2 \;=\; \int_0^1 \kappa^2(t)\;\sigma(t)\,\mathrm{d}t \;=\; 4\int_0^1 \frac{|\,\boldsymbol{\alpha}(t)\boldsymbol{\beta}'(t) - \boldsymbol{\alpha}'(t)\boldsymbol{\beta}(t)\,|^2}{(|\boldsymbol{\alpha}(t)|^2 + |\boldsymbol{\beta}(t)|^2)^3}\;\mathrm{d}t\,. \tag{46}$$

This defines the strain energy stored in an initially–straight elastic beam that is bent into the shape of a given space curve. As noted above, it is possible to evaluate (46) by a partial fraction expansion of the integrand if the roots of $\sigma(t)$ are known, but this can be rather cumbersome. However, it is possible to differentiate E with respect to the parameters w_i, w_f and evaluate the integrals in the resulting expressions by numerical quadrature.

The arc length S and the bending energy E both have shortcomings as measures to be minimized to identify interpolants of good shape. Curves for

which S is minimized may have regions of high curvature. On the other hand, curves for which E is minimized may have large arc lengths (for a circle of radius R, we note that $E = 2\pi/R \to 0$ while $S = 2\pi R \to \infty$ as $R \to \infty$). E may, in principle, be minimized under the constraint of a fixed value for S, but there is no *a priori* guarantee that the chosen value will admit solutions.

A weighted linear combination of S and E has been proposed as a shape measure that will penalize both high curvature and excessive arc length. But such a combination is not scale–invariant, since S has dimension `length` while E has dimension $(\texttt{length})^{-1}$. The product SE, on the other hand, is scale–independent: it depends only on the shape (not the size) of the curve.

6.2 Representative examples

Ideally, the interpolation would be formulated as a constrained optimization problem, in which some shape measure is minimized subject to satisfaction of the conditions (38)–(41) by the variables x_1, y_1, x_2, y_2 and w_i, w_f. However, developing robust and efficient algorithms for this is a substantive problem in its own right, which we defer to a future study.

The examples presented below were computed using a computer algebra system to solve the equations (38)–(41) numerically for given w_i, w_f values, and the system graphical display function was used to animate the behavior of these solutions as w_i, w_f are varied continuously. In this manner, a "visual" identification of parameter values that provide solutions with desirable shape properties was possible. It was observed that, as w_i, w_f are varied, either zero or two real solutions exist — or, exceptionally, two coincident real solutions. Because of their non–linear nature, it is difficult to verify that the equations (38)–(41) always admit real solutions for *some* w_i, w_f values, given arbitrary motion data. But the availability of these free parameters, and our experience with the numerical experiments, suggest that this is probable.

Examples 2–4 below re–visit the data used to construct RRMF quintic motion interpolants in [9]. Examples 2 and 3 show that, for suitable choices of w_i and w_f, one can obtain motion interpolants of shape quality comparable to, or better than, that of the RRMF quintics. Example 4 shows the possibility of interpolants to motion data for which the RRMF quintics admit no solution. Finally, Example 5 illustrates the interpolation of motion data sampled from a smooth analytic curve — a circular helix — for which closed–form (though not rational) expressions for the RMF vectors are known.

Example 2. The data for Example 1 in [9] comprises the displacement vector

$\Delta\mathbf{p} = (1, 0, 0)$ and initial/final frames specified by

$$(\mathbf{t}_i, \mathbf{u}_i, \mathbf{v}_i) \;=\; (\mathcal{Q}_0\,\mathbf{i}\,\mathcal{Q}_0^*,\, \mathcal{Q}_0\,\mathbf{j}\,\mathcal{Q}_0^*,\, \mathcal{Q}_0\,\mathbf{k}\,\mathcal{Q}_0^*)\,, \tag{47}$$

$$(\mathbf{t}_f, \mathbf{u}_f, \mathbf{v}_f) \;=\; (\mathcal{Q}_1\,\mathbf{i}\,\mathcal{Q}_1^*,\, \mathcal{Q}_1\,\mathbf{j}\,\mathcal{Q}_1^*,\, \mathcal{Q}_1\,\mathbf{k}\,\mathcal{Q}_1^*)\,, \tag{48}$$

where the unit quaternions $\mathcal{Q}_0$, $\mathcal{Q}_1$ are defined by

$$\mathcal{Q}_0 \;=\; (\cos\tfrac{1}{2}\phi_0 + \sin\tfrac{1}{2}\phi_0\,\mathbf{n}_0)\,\mathcal{S}\,, \qquad \mathcal{Q}_1 \;=\; (\cos\tfrac{1}{2}\phi_1 + \sin\tfrac{1}{2}\phi_1\,\mathbf{n}_1)\,\mathcal{S}\,,$$

with

$$\phi_0 \;=\; \frac{\pi}{4}\,, \quad \mathbf{n}_0 \;=\; (0, 0, 1) \qquad \text{and} \qquad \phi_1 \;=\; -\,\frac{\pi}{4}\,, \quad \mathbf{n}_1 \;=\; \frac{(1, 1, 1)}{\sqrt{3}}\,,$$

and $\mathcal{S} = (-1+\mathbf{i})/\sqrt{2}$. This data is reduced to canonical form, in the sense of Definition 1, by setting $(\mathbf{t}_i, \mathbf{u}_i, \mathbf{v}_i) = (\mathbf{i}, \mathbf{j}, \mathbf{k})$ and making the transformations

$$\Delta\mathbf{p} \;\to\; \mathcal{Q}_0^*\,\Delta\mathbf{p}\,\mathcal{Q}_0\,, \quad (\mathbf{t}_f, \mathbf{u}_f, \mathbf{v}_f) \;\to\; (\mathcal{Q}_0^*\,\mathbf{t}_f\,\mathcal{Q}_0,\, \mathcal{Q}_0^*\,\mathbf{u}_f\,\mathcal{Q}_0,\, \mathcal{Q}_0^*\,\mathbf{v}_f\,\mathcal{Q}_0)\,. \tag{49}$$

By visual inspection, the values $(w_i, w_f) = (1.01, -1.78)$ are found to yield a good solution. There are two distinct interpolants, defined by the coefficients

$$\begin{aligned}
\mathcal{A}_0 \;&=\; 1.010000\,,\\
\mathcal{A}_1 \;&=\; 1.102520 + 0.125786\,\mathbf{j} + 0.543737\,\mathbf{k}\,,\\
\mathcal{A}_2 \;&=\; 0.304785 + 0.337894\,\mathbf{j} + 0.085320\,\mathbf{k}\,,\\
\mathcal{A}_3 \;&=\; 1.368820 - 0.513842\,\mathbf{i} + 0.992666\,\mathbf{j} - 0.212840\,\mathbf{k}\,,
\end{aligned}$$

and

$$\begin{aligned}
\mathcal{A}_0 \;&=\; 1.010000\,,\\
\mathcal{A}_1 \;&=\; -\,0.952646 - 0.356107\,\mathbf{j} - 0.416772\,\mathbf{k}\,,\\
\mathcal{A}_2 \;&=\; 1.927890 + 0.369852\,\mathbf{j} + 0.918649\,\mathbf{k}\,,\\
\mathcal{A}_3 \;&=\; 1.368820 - 0.513842\,\mathbf{i} + 0.992666\,\mathbf{j} - 0.212840\,\mathbf{k}\,,
\end{aligned}$$

in (16). The arc length (44) and bending energy (46) for the first interpolant are $S = 1.19035$ and $E = 4.81259$, while for the second they are $S = 1.10768$ and $E = 54.1824$. Figure 1 shows the two interpolants, with a parallelepiped indicating the initial/final frame orientations. Also shown is an animation of the rotation–minimizing motions defined by them. Clearly, the first solution is preferable, as suggested by its lower bending energy. The second solution exhibits a small region of high curvature near one end, apparent in Figure 1.

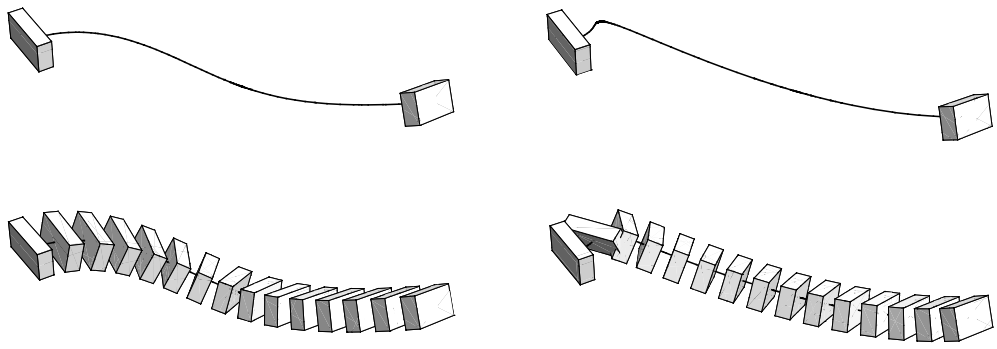

Figure 1: Upper: the degree 7 interpolants to the motion data of Example 2 — the parallelepiped indicates the initial and final frame orientations. Lower: animation of the rational rotation–minimizing motions defined by these two degree 7 interpolants. The motion has been discretized by uniform arc–length increments, corresponding to maintenance of uniform speed, along the path.

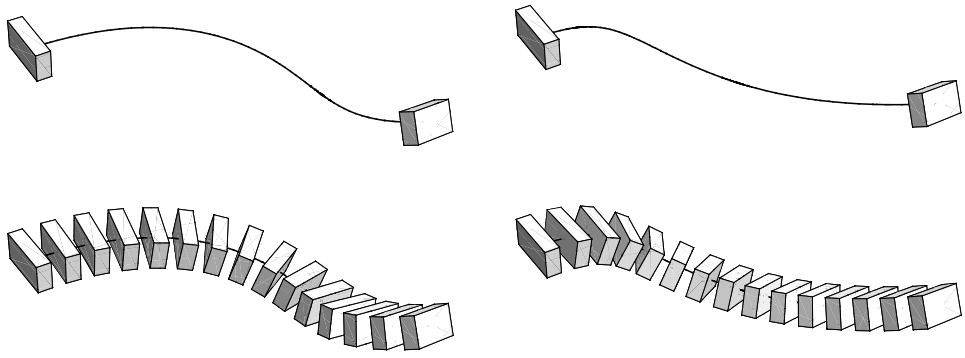

Figure 2: The two RRMF quintic interpolants to the Example 2 data, from [9], for comparison with the degree 7 interpolants with rotation–minimizing ERFs shown in Figure 1. Note that these rational RMFs are of degree 8, as compared to the degree 6 rational RMFs for the interpolants in Figure 1.

Two RRMF quintic interpolants to the motion data of this example were found in [9]. For comparison, they are shown in Figure 2. The first degree 7 rotation–minimizing ERF interpolant, at least, is of comparable shape quality to these RRMF quintic curves. This is apparent in the curvature plots shown in Figure 3. The other degree 7 interpolant should be rejected.

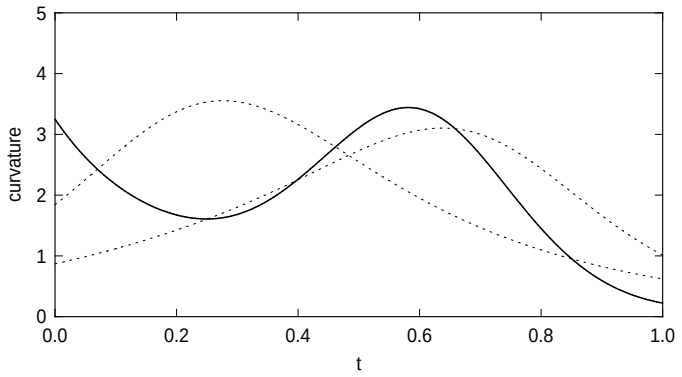

Figure 3: Comparison of the curvature plots for the first degree 7 rotation–minimizing ERF interpolant (solid line) and two RRMF quintic interpolants (dotted lines) from [9], for the spatial motion data specified in Example 2.

Example 3. For Example 2 in [9], $\Delta\mathbf{p} = (1, 0, 0)$ again, while $(\mathbf{t}_i, \mathbf{u}_i, \mathbf{v}_i)$ and $(\mathbf{t}_f, \mathbf{u}_f, \mathbf{v}_f)$ are defined as in the preceding example, with the choices

$$\phi_0 \,=\, \frac{\pi}{6}\,, \quad \mathbf{n}_0 \,=\, \frac{(0,1,2)}{\sqrt{5}} \qquad \text{and} \qquad \phi_1 \,=\, \frac{\pi}{3}\,, \quad \mathbf{n}_1 \,=\, \frac{(1,1,-2)}{\sqrt{6}}\,.$$

The data was reduced to canonical form as in the preceding example.

In this case, the parameter values $(w_i, w_f) = (1.39, 1.39)$ were found to give interpolants of good shape. For these values, two distinct solutions were obtained, with coefficients for (16) given by

$$\begin{aligned}
\mathcal{A}_0 \;&=\; 1.390000\,,\\
\mathcal{A}_1 \;&=\; 1.188430 - 0.073706\,\mathbf{j} - 0.613274\,\mathbf{k}\,,\\
\mathcal{A}_2 \;&=\; 0.291656 + 0.291452\,\mathbf{j} - 0.123586\,\mathbf{k}\,,\\
\mathcal{A}_3 \;&=\; 1.064230 + 0.405430\,\mathbf{i} + 0.793956\,\mathbf{j} + 0.069048\,\mathbf{k}\,,
\end{aligned}$$

and

$$\begin{aligned}
\mathcal{A}_0 &= 1.390000\,, \\
\mathcal{A}_1 &= 0.523536 - 0.221495\,\mathbf{j} - 0.286604\,\mathbf{k}\,, \\
\mathcal{A}_2 &= 0.988106 + 0.284614\,\mathbf{j} - 0.479820\,\mathbf{k}\,, \\
\mathcal{A}_3 &= 1.064230 + 0.405430\,\mathbf{i} + 0.793956\,\mathbf{j} + 0.069048\,\mathbf{k}\,.
\end{aligned}$$

The arc length and bending energy for the first interpolant are $S = 1.19619$ and $E = 5.38838$, while for the second they are $S = 1.17523$ and $E = 4.41097$. The interpolants are shown in Figure 4, in the same manner as in Figure 1. In this case the solutions are quite similar, as suggested by their arc lengths and bending energies (the second interpolant is perhaps somewhat preferable).

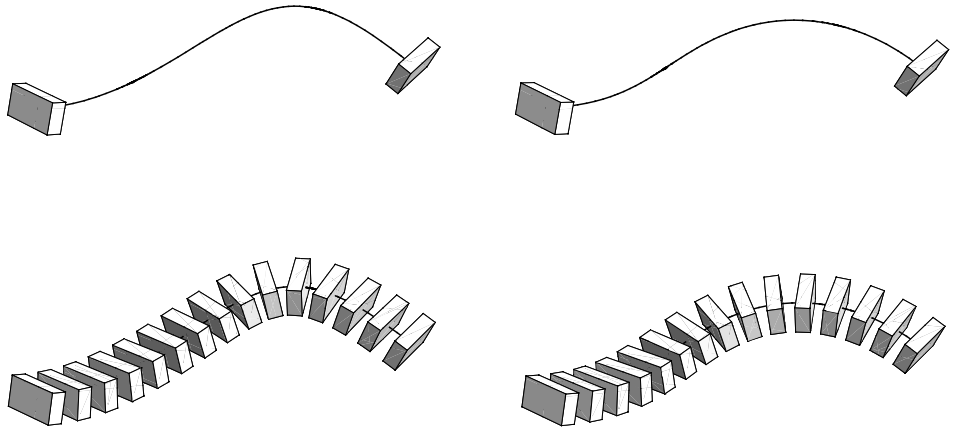

Figure 4: The two degree 7 interpolants to the motion data of Example 3.

Two distinct RRMF quintic interpolants were also found in [9] for this example, shown in Figure 5. By comparison of Figures 4 and 5, it is evident that the two degree 7 rotation–minimizing ERF interpolants and two RRMF quintic interpolants are all quite similar. Figure 6 compares the curvature plots for these two sets of motion interpolants.

Example 4. The data for Example 3 in [9] comprises the displacement vector $\Delta\mathbf{p} = (1, 0, 0)$ and initial/final frames defined by

$$\mathbf{t}_i = \frac{(1, 0, \sqrt{3})}{2}\,, \quad \mathbf{u}_i = (0, 1, 0)\,, \quad \mathbf{v}_i = \frac{(-\sqrt{3}, 0, 1)}{2}\,,$$

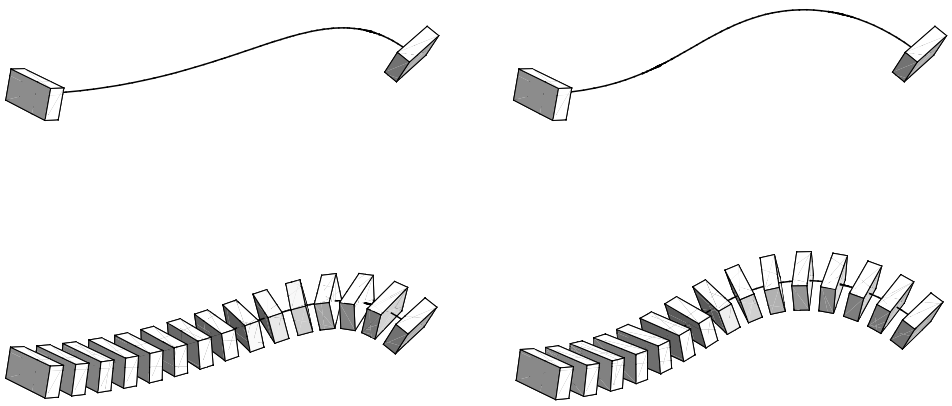

Figure 5: The two RRMF quintic interpolants to the Example 3 data from [9], for comparison with the corresponding degree 7 interpolants in Figure 1.

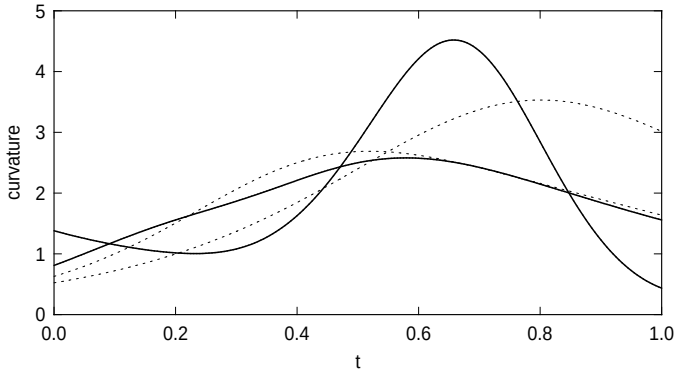

Figure 6: The curvature plots for the two degree 7 rotation–minimizing ERF interpolant (solid lines) compared with the two RRMF quintic interpolants (dotted lines) from [9], for the spatial motion data specified in Example 3.

$$\mathbf{t}_f \;=\; \frac{(1,-\sqrt{2},1)}{2}\,, \quad \mathbf{u}_f \;=\; \frac{(1,0,-1)}{\sqrt{2}}\,, \quad \mathbf{v}_f \;=\; \frac{(1,\sqrt{2},1)}{2}\,.$$

In this case, reduction to canonical form is achieved by setting $(\mathbf{t}_i, \mathbf{u}_i, \mathbf{v}_i) = (\mathbf{i}, \mathbf{j}, \mathbf{k})$ and invoking (49) with $\mathcal{Q}_0 = \frac{1}{2}(\sqrt{3} - \mathbf{j})$.

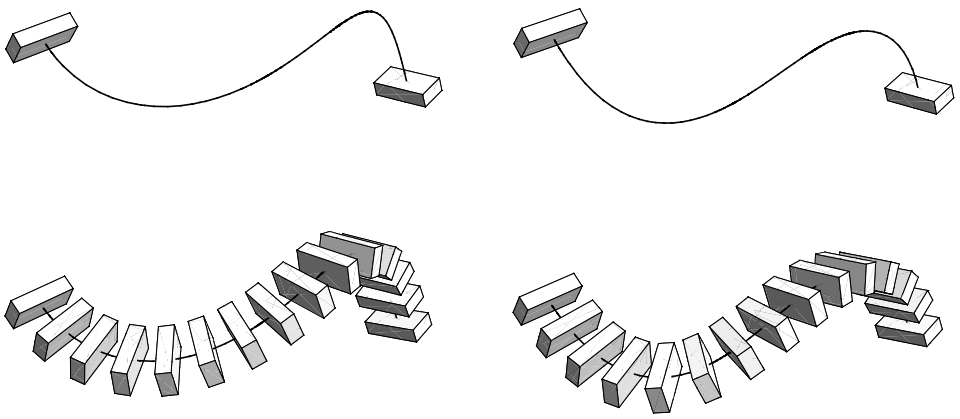

Figure 7: The two degree 7 interpolants to the motion data of Example 4.

In this case, the values $(w_i, w_f) = (1.52, -1.46)$ were found to yield good solutions, specified by the quaternion coefficients

$$\begin{aligned}
\mathcal{A}_0 &= 1.520000\,,\\
\mathcal{A}_1 &= 0.776903 + 1.166980\,\mathbf{j} + 0.896788\,\mathbf{k}\,,\\
\mathcal{A}_2 &= 0.181929 + 0.609912\,\mathbf{j} + 0.035746\,\mathbf{k}\,,\\
\mathcal{A}_3 &= 0.894064 - 0.997199\,\mathbf{i} + 0.516188\,\mathbf{j} - 0.267199\,\mathbf{k}\,,
\end{aligned}$$

and

$$\begin{aligned}
\mathcal{A}_0 &= 1.520000\,,\\
\mathcal{A}_1 &= 0.398324 + 0.378487\,\mathbf{j} + 0.573583\mathbf{k}\,,\\
\mathcal{A}_2 &= 0.630180 + 1.255390\,\mathbf{j} + 0.567579\,\mathbf{k}\,,\\
\mathcal{A}_3 &= 0.894064 - 0.997199\,\mathbf{i} + 0.516188\,\mathbf{j} - 0.267199\,\mathbf{k}\,.
\end{aligned}$$

The arc length and bending energy are $S = 1.35179$ and $E = 10.9894$ in the former case, and $S = 1.3554$ and $E = 10.559$ in the latter case. These values suggest that the motion interpolants are very similar, and this is corroborated by Figure 7. The curvature plots for the interpolants are shown in Figure 8.

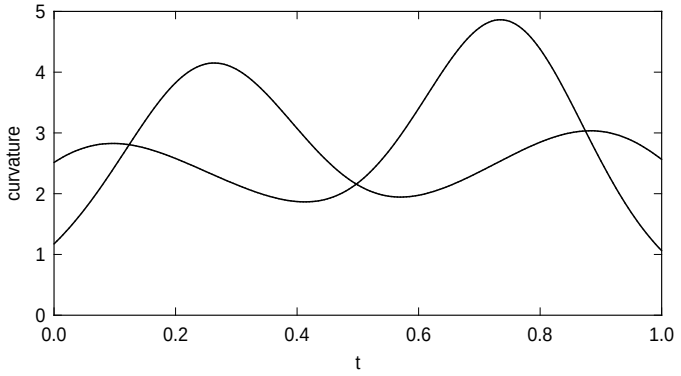

Figure 8: The curvature plots for the two degree 7 rotation–minimizing ERF interpolants to the spatial motion data specified in Example 4.

It was found in [9] that the data in this example does not admit RRMF quintic interpolants. Hence, degree 7 rotation–minimizing ERF interpolants may exist in cases where RRMF quintic interpolants are impossible.

Example 5. For the circular helix

$$\mathbf{r}(\phi) \;=\; (R\cos\phi, R\sin\phi, k\phi) \tag{50}$$

the Frenet frame can be written as

$$\mathbf{t} = (-a\,\sin\phi, a\cos\phi, b),\quad \mathbf{p} = (-\cos\phi, -\sin\phi, 0),\quad \mathbf{b} = (b\sin\phi, -b\cos\phi, a)$$

where $a = R/\sqrt{R^2+k^2}$ and $b = k/\sqrt{R^2+k^2}$, while the parametric speed, curvature, and torsion are

$$\sigma \;=\; \sqrt{R^2+k^2}\,,\quad \kappa \;=\; \frac{a}{\sigma}\,,\quad \tau \;=\; \frac{b}{\sigma}\,.$$

The deviation of the RMF normal–plane vectors $(\mathbf{u}, \mathbf{v})$ from the Frenet frame vectors $(\mathbf{p}, \mathbf{b})$ is thus

$$\theta \;=\; \theta_0 \;-\; \int_0^{\phi} \tau\,\sigma\,\mathrm{d}\phi \;=\; \theta_0 \;-\; b\,\phi\,.$$

Taking $\theta_0 = 0$, the RMF normal–plane vectors are

$$\begin{aligned}
\mathbf{u} \;&=\; (-\cos\phi\cos b\phi - b\sin\phi\sin b\phi, -\sin\phi\cos b\phi + b\cos\phi\sin b\phi, -a\sin b\phi)\,,\\
\mathbf{v} \;&=\; (-\cos\phi\sin b\phi + b\sin\phi\cos b\phi, -\sin\phi\sin b\phi - b\cos\phi\cos b\phi, a\cos b\phi)\,.
\end{aligned}$$

Choosing $R = \sqrt{3}$ and $k = 1$, we obtain $a = \frac{1}{2}\sqrt{3}$ and $b = \frac{1}{2}$. For end points defined by $\phi_i = 0$, $\phi_f = \frac{1}{2}\pi$ we have $\Delta\mathbf{p} = (-\sqrt{3}, \sqrt{3}, \frac{1}{2}\pi)$ and

$$\mathbf{t}_i \;=\; \tfrac{1}{2}(0, \sqrt{3}, 1)\,, \quad \mathbf{u}_i \;=\; (-1, 0, 0)\,, \quad \mathbf{v}_i \;=\; \tfrac{1}{2}(0, -1, \sqrt{3})\,,$$

$$\mathbf{t}_f \;=\; \tfrac{1}{2}(-\sqrt{3}, 0, 1)\,, \quad \mathbf{u}_f \;=\; \tfrac{1}{4}(-\sqrt{2}, -2\sqrt{2}, -\sqrt{6})\,, \quad \mathbf{v}_f \;=\; \tfrac{1}{4}(\sqrt{2}, -2\sqrt{2}, \sqrt{6})\,.$$

The initial frame is generated through (47) using the quaternion

$$\mathcal{Q}_0 \;=\; \frac{(2\,\mathbf{i} + \sqrt{3}\,\mathbf{j} + \mathbf{k})}{2\sqrt{2}}\,(\cos\tfrac{1}{2}\phi_0 + \sin\tfrac{1}{2}\phi_0\,\mathbf{i})\,, \quad \phi_0 = \frac{7\pi}{8}\,.$$

Reduction to canonical form is thus achieved by setting $(\mathbf{t}_i, \mathbf{u}_i, \mathbf{v}_i) = (\mathbf{i}, \mathbf{j}, \mathbf{k})$ and invoking (49) with $\mathcal{Q}_0$ as defined above.

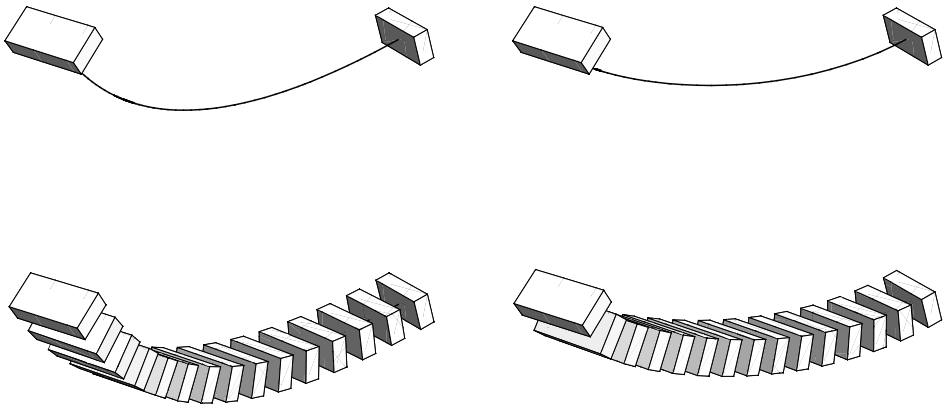

Figure 9: Degree 7 interpolants to positions and rotation–minimizing frames sampled at $\phi = 0$ and $\frac{1}{2}\pi$ from the circular helix (50) with $R = \sqrt{3}$, $k = 1$.

For the values $(w_i, w_f) = (1.14, 2.35)$ two solutions were obtained, with quaternion coefficients

$$\begin{aligned}
\mathcal{A}_0 \;&=\; 1.140000\,,\\
\mathcal{A}_1 \;&=\; 1.636390 + 0.099096\,\mathbf{j} + 0.152096\,\mathbf{k}\,,\\
\mathcal{A}_2 \;&=\; 1.901260 - 0.012749\,\mathbf{j} + 0.485457\,\mathbf{k}\,,\\
\mathcal{A}_3 \;&=\; 1.853160 + 0.131700\,\mathbf{i} - 0.550710\,\mathbf{j} + 1.329530\,\mathbf{k}\,,
\end{aligned}$$

and

$$\begin{aligned}
\mathcal{A}_0 &= 1.14000\,, \\
\mathcal{A}_1 &= -1.711400 - 0.030904\,\mathbf{j} - 0.334667\,\mathbf{k}\,, \\
\mathcal{A}_2 &= 4.425560 + 0.202195\,\mathbf{j} + 0.570214\,\mathbf{k}\,, \\
\mathcal{A}_3 &= 1.853160 + 0.131700\,\mathbf{i} - 0.550710\,\mathbf{j} + 1.329530\,\mathbf{k}\,.
\end{aligned}$$

The arc length and bending energy are $S = 3.14512$ and $E = 0.610073$ for the former case, $S = 3.04441$ and $E = 10.9288$ for the latter. The interpolants are illustrated in Figure 9. The large energy for the latter solution is due to a small high–curvature region near one end of the interpolant, that is difficult to discern in Figure 9 — this solution should be rejected. The first solution, on the other hand, approximates the helical arc quite well. Figure 10 illustrates the curvature and torsion plots for this solution. The curvature conforms well to the value for the exact helix, although the torsion is initially higher. The interpolant remains close to the exact helix segment over its entire extent.

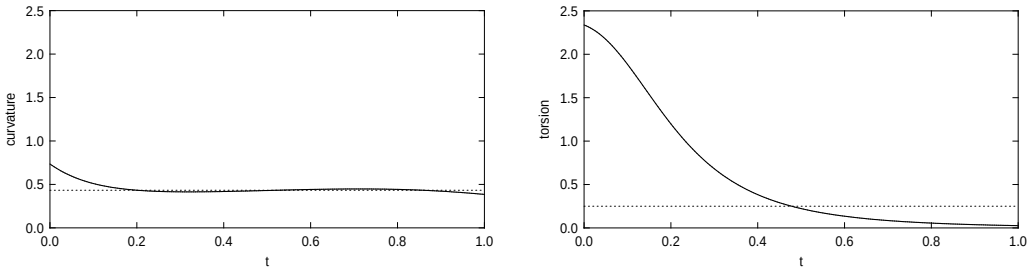

Figure 10: The curvature (left) and torsion (right) plots for the first degree 7 rotation–minimizing ERF interpolant to motion data sampled from a helix in Example 5. Dotted lines show the curvature and torsion of the exact helix.

For general input data, the complexity of equations (38)–(41) precludes a simple proof of the existence of solutions for *some* values of the parameters w_i, w_f. Instead, we give empirical evidence suggesting that this may be true. For the displacement vector[5] $\Delta\mathbf{p} = (1, 0, 0)$ a total of 1000 pairs of randomly–oriented end frames $(\mathbf{t}_i, \mathbf{u}_i, \mathbf{v}_i)$ and $(\mathbf{t}_f, \mathbf{u}_f, \mathbf{v}_f)$ were chosen. For each pair of end frames w_i, w_f values were chosen randomly from the interval $[\,-10, +10\,]$. If no solution was obtained with the chosen values, the process was repeated with newly–chosen w_i, w_f values, up to a maximum of 100 times.

[5]Note that, by Remark 4, fixing $|\Delta\mathbf{p}|$ does not influence the existence of solutions.

Figure 11 shows a histogram of the number of input data sets that yielded a solution within a given number of w_i, w_f choices. The vast majority of cases yield a solution within just a few choices. In particular, 491 cases produced a solution with the first random choices for w_i, w_f on the interval $[\,-10, +10\,]$. Note the "tail" in the distribution (32 cases) evident in Figure 11 — for these cases, no solution was obtained within 100 random w_i, w_f choices. This may be an artifact of restricting the two free parameters to the interval $[\,-10, +10\,]$ rather than an indication of non–existence of solutions. In principle, it can be remedied by employing a larger interval, but this distorts the distribution under uniform sampling, since most solutions occur for small w_i, w_f values, which become more sparsely sampled when the range is increased.

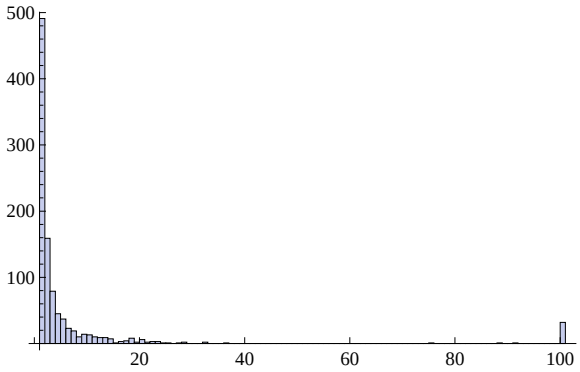

Figure 11: Histogram showing number of data sets (vertical axis) for which a solution was found within a given number of w_i, w_f choices (horizontal axis).

7 Closure

A characterization of the degree 7 spatial PH curves with rotation–minimizing Euler–Rodrigues frames has been derived, and used to formulate the problem of identifying a rational rotation–minimizing rigid–body motion interpolant to given initial/final positions and frames $\mathbf{p}_i$, $(\mathbf{t}_i, \mathbf{u}_i, \mathbf{v}_i)$ and $\mathbf{p}_f$, $(\mathbf{t}_f, \mathbf{u}_f, \mathbf{v}_f)$ as a system of four quadratic equations in four real variables. These equations, containing two free parameters that control the magnitudes of the interpolant end–derivatives, are well–conditioned and amenable to accurate solution by numerical methods. Computed examples show that motion interpolants with excellent shape properties can be obtained through appropriate choices of the free parameters, and solutions exist for data sets that do not admit a quintic

RRMF interpolant. Moreover, the rational RMFs on these new interpolants are of degree 6, rather than degree 8 for the RRMF quintics in [9].

The goals of this paper were to characterize the degree 7 PH curves with rotation–minimizing ERFs in a manner amenable to the motion interpolation problem; to formulate a system of equations that embodies this problem; and to demonstrate the existence of solutions with excellent shape properties for suitable choices of the two free parameters. The systematic exploitation of these free parameters, in terms of optimizing certain integral shape measures, is a substantive open problem that we defer to a future study.

References

[1] R. L. Bishop (1975), There is more than one way to frame a curve, *Amer. Math. Monthly* **82**, 246–251.

[2] H. I. Choi and C. Y. Han (2002), Euler–Rodrigues frames on spatial Pythagorean–hodograph curves, *Comput. Aided Geom. Design* **19**, 603–620.

[3] H. I. Choi, D. S. Lee, and H. P. Moon (2002), Clifford algebra, spin representation, and rational parameterization of curves and surfaces, *Adv. Comp. Math.* **17**, 5–48.

[4] R. T. Farouki (2008), *Pythagorean–Hodograph Curves: Algebra and Geometry Inseparable*, Springer, Berlin.

[5] R. T. Farouki (2010), Quaternion and Hopf map characterizations for the existence of rational rotation–minimizing frames on quintic space curves, *Adv. Comp. Math.* **33**, 331–348.

[6] R. T. Farouki, M. al–Kandari, and T. Sakkalis (2002), Structural invariance of spatial Pythagorean hodographs, *Comput. Aided Geom. Design* **19**, 395–407.

[7] R. T. Farouki, M. al–Kandari, and T. Sakkalis (2002), Hermite interpolation by rotation–invariant spatial Pythagorean–hodograph curves, *Adv. Comp. Math.* **17**, 369–383.

[8] R. T. Farouki, C. Giannelli, C. Manni, and A. Sestini (2009), Quintic space curves with rational rotation–minimizing frames, *Comput. Aided Geom. Design* **26**, 580–592.

[9] R. T. Farouki, C. Giannelli, C. Manni, and A. Sestini (2012), Design of rational rotation–minimizing rigid body motions by Hermite interpolation, *Math. Comp.* **81**, 879–903.

[10] R. T. Farouki, C. Giannelli, and A. Sestini (2009), Helical polynomial curves and double Pythagorean hodographs I. Quaternion and Hopf map representations, *J. Symb. Comput.* **44**, 161–179.

[11] R. T. Farouki and C. Y. Han (2003), Rational approximation schemes for rotation–minimizing frames on Pythagorean–hodograph curves, *Comput. Aided Geom. Design* **20**, 435–454.

[12] R. T. Farouki and T. Sakkalis (2012), A complete classification of quintic space curves with rational rotation–minimizing frames, *J. Symb. Comput.* **47**, 214–226

[13] C. Y. Han (2008), Nonexistence of rational rotation–minimizing frames on cubic curves, *Comput. Aided Geom. Design* **25**, 298–304.

[14] F. Klok (1986), Two moving coordinate frames for sweeping along a 3D trajectory, *Comput. Aided Geom. Design* **3**, 217–229.

[15] M. Krajnc and V. Vitrih (2012), Motion design with Euler–Rodrigues frames of quintic Pythagorean–hodograph curves, *Math. Comput. Simul.* **82**, 1696–1711.

[16] Z. Sir and B. Jüttler (2005), Spatial Pythagorean hodograph quintics and the approximation of pipe surfaces, in *Mathematics of Surfaces XI* (R. Martin, H. Bez, and M. Sabin, eds.) Springer, Berlin, pp. 364–380.

[17] W. Wang and B. Joe (1997), Robust computation of the rotation minimizing frame for sweep surface modelling, *Comput. Aided Design* **29**, 379–391.

[18] W. Wang, B. Jüttler, D. Zheng, Y. Liu (2008), Computation of rotation minimizing frames, *ACM Trans. Graphics* **27**, No. 1, Article 2, 1–18.